



Transportation Consortium of South-Central States

Solving Emerging Transportation Resiliency, Sustainability, and Economic Challenges through the Use of Innovative Materials and Construction Methods: From Research to Implementation

Resilient 3D-Printed Infrastructure with Engineered Cementitious Composites (ECC)

Project No. 20CUNM41

Lead University: University of New Mexico

**Final Report
August 2021**

Disclaimer

The contents of this report reflect the views of the authors, who are responsible for the facts and the accuracy of the information presented herein. This document is disseminated in the interest of information exchange. The report is funded, partially or entirely, by a grant from the U.S. Department of Transportation's University Transportation Centers Program. However, the U.S. Government assumes no liability for the contents or use thereof.

Acknowledgements

The authors gratefully acknowledge the financial support from the Tran Set under Award # 20CUNM05. Any opinions, findings and conclusions or recommendations expressed in this material are those of the authors and do not reflect the views of the Tran Set view. The authors would like to thank for the invaluable assistance of Ms. Michele Anderson in laboratory work. All tests were performed in the Dana C. Wood Materials and Structures Lab at UNM

TECHNICAL DOCUMENTATION PAGE

1. Project No. 20CUNM41	2. Government Accession No.	3. Recipient's Catalog No.	
4. Title and Subtitle Resilient 3D-Printed Infrastructure with Engineered Cementitious Composites (ECC)		5. Report Date Aug. 2021	
7. Author(s) PI: Maryam Hojati ORCID – 0000-0001-6043-7173		6. Performing Organization Code	
9. Performing Organization Name and Address Transportation Consortium of South-Central States (Tran-SET) University Transportation Center for Region 6 3319 Patrick F. Taylor Hall, Louisiana State University, Baton Rouge, LA 70803		8. Performing Organization Report No.	
12. Sponsoring Agency Name and Address United States of America Department of Transportation Research and Innovative Technology Administration		10. Work Unit No. (TRAIS)	
		11. Contract or Grant No. 69A3551747106	
15. Supplementary Notes Report uploaded and accessible at Tran-SET's website (http://transet.lsu.edu/) .		13. Type of Report and Period Covered Final Research Report Aug. 2020 – Aug. 2021	
		14. Sponsoring Agency Code	
16. Abstract Conventional construction of reinforced concrete structures is slow, labor-intensive, and expensive. 3D printing holds great potential to assist engineers and architects in constructing fast and economical yet complex representational infrastructures. One of the most significant barriers to the broader adoption of concrete 3D printing in civil infrastructure is the difficulty of providing printed structural components with reinforcement to achieve sound structural performance under different loading conditions. Hence, it is essential to design concrete that can be utilized as a rebar-free material by considering strength and ductility. Recently, the development of Engineered Cementitious Composites (ECC) has neared the possibility to achieve both strength and ductility in the concrete structures without embedding steel reinforcement. ECC has been offered to enhance the problem related to the ductility and low tensile strength of traditional concrete and Fiber Reinforced Composite (FRC). As such, the implementation of intrinsically reinforced cementitious materials has the potential to address this barrier in the reinforcement of 3D-printed concrete and yields significant benefits such as an enhanced structural capacity, durability, and resiliency. This project proposes the development of ECC materials utilizing readily available ingredients in Region 6 with rheological characteristics tailored specifically for 3D printing applications. Furthermore, the project aims to conduct a comprehensive evaluation of the hardened properties of 3D-printed ECC specimens, including mechanical tests.			
17. Key Words Engineered Cementitious Composites, Ductility, Strength, 3-D Printing, Concrete Construction, Supplementary Cementitious Materials		18. Distribution Statement No restrictions. This document is available through the National Technical Information Service, Springfield, VA 22161.	
19. Security Classif. (of this report) Unclassified	20. Security Classif. (of this page) Unclassified	21. No. of Pages 45	22. Price

Form DOT F 1700.7 (8-72)

Reproduction of completed page authorized.

SI* (MODERN METRIC) CONVERSION FACTORS

APPROXIMATE CONVERSIONS TO SI UNITS

Symbol	When You Know	Multiply By	To Find	Symbol
LENGTH				
in	inches	25.4	millimeters	mm
ft	feet	0.305	meters	m
yd	yards	0.914	meters	m
mi	miles	1.61	kilometers	km
AREA				
in ²	square inches	645.2	square millimeters	mm ²
ft ²	square feet	0.093	square meters	m ²
yd ²	square yard	0.836	square meters	m ²
ac	acres	0.405	hectares	ha
mi ²	square miles	2.59	square kilometers	km ²
VOLUME				
fl oz	fluid ounces	29.57	milliliters	mL
gal	gallons	3.785	liters	L
ft ³	cubic feet	0.028	cubic meters	m ³
yd ³	cubic yards	0.765	cubic meters	m ³
NOTE: volumes greater than 1000 L shall be shown in m ³				
MASS				
oz	ounces	28.35	grams	g
lb	pounds	0.454	kilograms	kg
T	short tons (2000 lb)	0.907	megagrams (or "metric ton")	Mg (or "t")
TEMPERATURE (exact degrees)				
°F	Fahrenheit	5 (F-32)/9 or (F-32)/1.8	Celsius	°C
ILLUMINATION				
fc	foot-candles	10.76	lux	lx
fl	foot-Lamberts	3.426	candela/m ²	cd/m ²
FORCE and PRESSURE or STRESS				
lbf	poundforce	4.45	newtons	N
lbf/in ²	poundforce per square inch	6.89	kilopascals	kPa
APPROXIMATE CONVERSIONS FROM SI UNITS				
Symbol	When You Know	Multiply By	To Find	Symbol
LENGTH				
mm	millimeters	0.039	inches	in
m	meters	3.28	feet	ft
m	meters	1.09	yards	yd
km	kilometers	0.621	miles	mi
AREA				
mm ²	square millimeters	0.0016	square inches	in ²
m ²	square meters	10.764	square feet	ft ²
m ²	square meters	1.195	square yards	yd ²
ha	hectares	2.47	acres	ac
km ²	square kilometers	0.386	square miles	mi ²
VOLUME				
mL	milliliters	0.034	fluid ounces	fl oz
L	liters	0.264	gallons	gal
m ³	cubic meters	35.314	cubic feet	ft ³
m ³	cubic meters	1.307	cubic yards	yd ³
MASS				
g	grams	0.035	ounces	oz
kg	kilograms	2.202	pounds	lb
Mg (or "t")	megagrams (or "metric ton")	1.103	short tons (2000 lb)	T
TEMPERATURE (exact degrees)				
°C	Celsius	1.8C+32	Fahrenheit	°F
ILLUMINATION				
lx	lux	0.0929	foot-candles	fc
cd/m ²	candela/m ²	0.2919	foot-Lamberts	fl
FORCE and PRESSURE or STRESS				
N	newtons	0.225	poundforce	lbf
kPa	kilopascals	0.145	poundforce per square inch	lbf/in ²

TABLE OF CONTENTS

TECHNICAL DOCUMENTATION PAGE	ii
TABLE OF CONTENTS.....	iv
LIST OF FIGURES	vi
LIST OF TABLES	viii
ACRONYMS, ABBREVIATIONS, AND SYMBOLS	ix
EXECUTIVE SUMMARY	x
1. INTRODUCTION	1
2. OBJECTIVES.....	2
3. LITERATURE REVIEW	3
4. METHODOLOGY	5
4.1. Material and Mix Design	5
4.2. Mixing Procedure and Test Methods.....	7
4.3. 3D-Printing System.....	7
4.4. Pretests	8
4.4.1. Setting time test.....	8
4.4.2. Flow table test	9
4.5. Rheology	9
4.6. 3D-printing Tests	10
4.6.1. Extrudability	10
4.6.2. Buildability	11
4.7. Mechanical Properties.....	12
4.7.1. Compressive strength test (Cast Specimens)	12
4.7.2. Direct tension test	12
4.7.3. Compressive strength tests (Printed Specimens)	13
4.7.4. Beam tests (3D Printed)	14
5. ANALYSIS AND FINDINGS	16
5.1. Fresh Properties	16
5.1.1. Flow Table Test Results.....	16
5.1.2. Rheology	16

5.2. Printability	21
5.2.1. Extrudability	21
5.2.2. Buildability	27
5.3. Mechanical Properties.....	29
5.3.1. Compressive Strength (Cast Specimens)	29
5.3.2. Compressive Strength (3D printed specimens).....	32
5.3.3. Dry Density	32
5.3.4. Direct Tension Test.....	33
5.3.5. Flexural Strength.....	33
5.3.6. Fracture Properties	34
6. CONCLUSIONS.....	35
REFERENCES	36
APPENDIX A: Technical Parameters of 3D-Printer	41

LIST OF FIGURES

Figure 1. Particle size distribution (Gradation) of River Sand	5
Figure 2. UNM Dana C. Wood Materials and Structures Lab 3D-Printing Systems (a) 3D-Printing of Concrete (b) 3D-Printing of Clay	7
Figure 3. Vicat needle test	8
Figure 4. Flow table test.....	9
Figure 5. (a) Brookfield Rheometer RST-SST (b) Hysteresis loop testing profile	10
Figure 6. The experimental approach to measuring plastic viscosity, yield stress, and thixotropy adopts the Bingham model.	10
Figure 7. 60 x 60 cm 3D-printed hollow square for the extrudability evaluation	11
Figure 8. 3D-printed wall for the buildability evaluation	12
Figure 9. (a) Uniaxial direct tension test setup, (b) specimens dimension according to JSCE recommendations, (c) casted dog-bone sample	13
Figure 10. (a) Testing direction and cutting diagram of four cubic samples extracted from 150×150×60mm primary prism sample, (b) primary prism sample, (c) four extracted 50×50×50mm cubic samples from the primary sample.	14
Figure 11. (a) Three-point bending test setup, (b) 3D-Printed beam, (c) designed beam using 3D software.....	15
Figure 12. Hysteresis curves of ECC mixtures.....	17
Figure 13. Plastic viscosity and yield stress of ECC mixtures (Linear fits are used to measure). 17	
Figure 14. Plastic Viscosity of standard ECC mixes	18
Figure 15. Plastic Viscosity of ECC mixes with MC	18
Figure 16. Static Yield Stress of standard ECC mixes	19
Figure 17. Static Yield Stress of ECC mixes with MC.....	19
Figure 18. Dynamic Yield Stress of standard ECC mixes.....	20
Figure 19. Dynamic Yield Stress of ECC mixes with MC.....	20
Figure 20. Thixotropy of standard ECC mixes	21
Figure 21. Thixotropy of ECC mixes with MC	21
Figure 22. Cross-sections of walls printed for buildability evaluation (left to right) (a) at 0 minutes time gap (b) at 5 minutes time gap	27
Figure 23. Compressive strength of standard ECC mixtures at 7, 14, and 28 days.....	30
Figure 24. Compressive strength of MC-rich ECC mixtures at 7, 14, and 28 days	30

Figure 25. Compressive strength of 75% cement replacement with FA, S, and SF.....	31
Figure 26. Compressive strength of the Primary mixtures.	31
Figure 27. 28 days Compressive strength of the 3D printed specimens.....	32
Figure 28. Deflection at the peak strength.....	33
Figure 29. Peak strength of 3D-printed beams.....	34
Figure 30. Single crack of the beam samples under flexural load.	34

LIST OF TABLES

Table 1. Chemical composition of cementitious dry powders.....	5
Table 2. Mix design of different ECC mixtures	6
Table 3. Flow table results of standard ECC mixtures.	16
Table 4. Flow table results of ECC mixtures containing MC.....	16
Table 5. Extrudability evaluation results at 1 cm/s printing speed.....	23
Table 6. Extrudability evaluation results at 2 cm/s printing speed.	24
Table 7. Extrudability evaluation results at 4 cm/s printing speed.	25
Table 8. Extrudability evaluation results at 5 cm/s printing speed.	26
Table 9. Buildability evaluation of different ECC mixtures.....	28
Table 10. Preliminary compressive strength results according to ASTM C39.....	29
Table 11. Dry Density of ECC specimens	32
Table 12. Preliminary compressive strength results according to ASTM C39.....	33

ACRONYMS, ABBREVIATIONS, AND SYMBOLS

AM	Additive Manufacturing
ECC	Engineered Cementitious Composites
3D	Three Dimensional
C	Cement
FA	Fly Ash
S	Slag
MK	Metakaolin
SF	Silica Fume
W	Water
RS	River Sand
B	Binder
HRWR	High Range Water Reducer
MC	Methyl Cellulose
VMA	Viscosity Modifying Admixture

EXECUTIVE SUMMARY

Additive manufacturing (AM), also known as 3D printing, enables the manufacturing of complex three-dimensional shapes and structures that are rendered as digital models through 3D modeling software or by importing a 3D scan of an object into the 3D modeling software. The flexibility of AM for producing industrial products is revolutionizing all manufacturing processes and is claimed to be the fourth industrial revolution. AM can also assist engineers and architects in the production of fast and economical yet complex representational models during the design phase to simulate and study the designed object. Printing freeform structures in the building industry results in higher precision, safer working conditions, faster construction speed, and lower costs of construction (avoiding the costs associated with formwork and labor). To make these benefits a reality, research focused on the 3D printing of concrete is rapidly gaining more attention. One of the biggest barriers to the broader adoption of concrete 3D printing in civil infrastructure is the difficulty of providing printed structural components with reinforcement to achieve sound structural performance under different loading conditions.

Concrete is the most largely used construction material in the world. Concrete materials exhibit two well-documented weaknesses, which are their low tensile strength and highly brittle nature. As such, concrete materials rely on steel reinforcement to produce sound structural members ensuring sufficient tensile load carrying capacity, safety, and reliability. While steel reinforcement is fundamental for the structural performance of reinforced concrete elements, steel rebar is the main cause of reinforced concrete structures deterioration due to the action of corrosion. In turn, steel rebar significantly limits the durability potential of modern infrastructure. For instance, iconic Roman buildings such as the Pantheon (built without steel reinforcement) are still standing after nearly two thousand years; yet, modern reinforced-concrete structures have a hard time exhibiting durability of one hundred years or greater. The durability problem of modern infrastructure is one of the most important challenges to be solved by scientists and engineers over the next decades. One potential solution to this problem is to provide new concrete materials exhibiting high tensile strength and ductility, which can eliminate the need for rebar. As such, rebar-free structures could eliminate the corrosion deterioration mechanism and allow for dramatic durability enhancements. In addition, the absence of steel reinforcement could lead to a substantial increase in construction productivity as the rebar placement activity (which is a highly time-consuming process) would no longer be required. Moreover, such a material would be ideal to be utilized with emerging construction technics such as 3D printing, where the inclusion of steel reinforcement is not possible.

Recently, the development of Engineered Cementitious Composites (ECC) has neared the possibility of achieving structurally sound rebar-free concrete structures. ECCs are a novel type of concrete materials that achieves high strength (i.e., >120 MPa compressive strength and >17 MPa tensile strength) and high ductility (i.e., >8% tensile strain capacity) by combining the micromechanics and fracture mechanics design concepts of ECC and the high particle packing density matrix design approach of UHPC. As such, this research project aims to develop novel ECC materials utilizing readily available ingredients in Region 6. The development of such materials will provide the region with state-of-the-art cementitious composites that will be available for the repair and new construction of transportation infrastructure. Furthermore, this study investigates the feasibility of manufacturing 3D-printed structures utilizing ECC materials.

This research characterizes the fresh and hardened properties of eight ECC mixtures and quantifies these materials' fresh properties to be used for 3D printing projects. This study identifies the influence of using different types of admixtures, including fly ash, slag, metakaolin, and silica fume, in ECC printing. 1.5% fiber was used in the ECC mixtures, but the quality of 3D-printed specimens with fibers indicated that the high content of the fibers lowers the quality of 3D-printed ECC specimens. The viscosity modifying admixture (VMA) was added to improve the quality of the 3D-printed ECC. The incorporation of methylcellulose as a VMA promoted fibers' dispersion and significantly improved printing quality in dimension conformity, dimension consistency, and shape retention of the printed objects. However, the addition of methylcellulose reduces the mechanical performance of ECC such as the compressive strength. The rheological parameters such as plastic viscosity, yield stress, and thixotropy of ECC mixtures with methylcellulose were marginally enhanced, another cause of improving extrudability and buildability

1. INTRODUCTION

Engineered Cementitious Composites (ECC) is a class of Ultra-high-performance concrete (UHPC) that was developed some decades ago by Dr. Victor Li, and since then, both material design and application have been revolutionized significantly. ECC was designed in response to the issues related to the brittleness of conventional concrete and quasi-brittleness of Fiber-Reinforced Cementitious Composite (FRC) (1-3).

ECC was designed on the basis of the micromechanics and fracture mechanics principles by using low-fiber contents (i.e., (to 2%) of short-fiber cementitious composites, and for this innovative composite material, a ductile failure mode with a large strain capacity was observed (4-6). This material exhibited superior mechanical properties (i.e., high tensile ductility, tight crack width, large strength both in tension and compression, low shrinkage, and creep), with self-healing characteristics that can effectively improve the durability of this material. The tensile ductility of ECC is about 200 to 500 times that of regular concrete or FRC (2 to 5% strain capacity in tension). The crack width in ECC is usually less than 100 micrometers during strain-hardening, which is noticeably smaller than the size of cracks in FRC and conventional concrete (7, 8). Furthermore, this material is significantly strong against foremost types of deterioration occurring in the concrete structures, including alkali-silica reaction, sulfate attack, freeze and thaw, and corrosion (7). The ECC design is according to the micromechanics and fracture mechanics theory, and development of an ECC mixture needs thoroughly engineering design and control in different scales of ECC material, including nano-, micro-, macro-and composite scales (8, 9). For the mixture designed for ECC, the size of the fiber, fineness of sand, toughness and flaw size of the matrix, chemical and frictional bonds in the interface of different components, strain hardening characteristics, tensile strength, and toughness should be controlled (8-10).

Since ECC was introduced, there has been substantial development in material design and commercial application, including structures, repair, and retrofit. One of the new areas for using ECC is in additive manufacturing to 3-D print robust infrastructures. This research project involves designing and developing a novel ECC where can be used in the 3D printing of concrete structures by utilizing readily available ingredients in Region 6. This study offered the region with the most recent stage in developing these novel cementitious composites that will be available for the structures, repair, and retrofit of transportation infrastructure. Furthermore, the feasibility of 3D printing of ECC materials for digital construction was evaluated.

2. OBJECTIVES

The objective of this research project involves the design and development of novel ECC where can be used in 3D printing of concrete structures by utilizing readily available ingredients in Region 6. This study offers the region with the most recent stage in developing these novel cementitious composites that are available for the structures, repair, and retrofit of transportation infrastructure. Furthermore, the feasibility of 3D printing of ECC materials for digital construction was evaluated through different tests, including compressive strength, setting time, flow table test, extrudability, buildability, rheology, and mechanical performance of 3D-printed specimens. This study shows the effective admixtures that could be used for 3D printing of ECC materials.

3. LITERATURE REVIEW

Additive manufacturing (AM), also known as 3D-printing, of cementitious materials has a high capacity to develop automation in the construction industry (Chaves Figueiredo et al., 2019). There are some challenges in applying AM in the 3D-printing of concrete materials, limiting the broad application of these innovative techniques in the construction industry. Incorporating reinforcing components, cold joint formation between layers, durability, and fresh properties of cementitious mixtures are some of the challenges. Over the last few years, some of these engineering challenges, specifically the fresh characteristics of cementitious mixtures and processing parameters, have been studied and addressed in numerous technical papers (Soltan and Li 2018, Roussel 2018, Roussel et al. 2020, Albar et al. 2020, Kazemian et al. 2017, Perrot et al. 2012, Weng et al. 2019, Wolfs et al. 2018). The previous research showed that novel 3D printing techniques must be engineered and customized according to the fresh property requirements (18).

Concrete is a brittle material and possesses a low tensile strength (i.e., less than 10 percent of compressive strength), which causes the occurrence and propagation of cracks due to load or changing environmental conditions (19). While the evolution of concrete strength, durability performance, and material greenness each address a particular need, adopting a comprehensive approach is crucial. Engineered Cementitious Composites (ECC) are a novel class of high-performance fiber-reinforced cementitious composites designed and optimized to exhibit a high tensile ductility (20). The emergence of ECC presented a comprehensive solution that possesses characteristics that support infrastructure resilience, durability, sustainability, and reduction of operations and maintenance needs simultaneously (19).

ECC materials are known for outstanding properties, such as high ductility varied from 3-7%, tight crack width around 60 μ m, and low fiber content of to 2% volume fraction (21). The reason to categorize the ECC as a strain-hardening material is similar to ECC and metal performances when subjected to external loads. The ECC specimens continue to bear the load after the emergence of the first crack resulting from the fiber and matrix interaction (Li 1992 and Yang et al. 2008). Furthermore, the compressive strength of ECCs also has a vital role in the capability of cementitious matters, especially for the structural elements, to sustain the human-induced load during their service life. Ranade (24) emphasized in his research study the existence of a balance between the compressive strength and tensile strength to achieve a high strength composite (HSC) and high ductility concrete (HDC) simultaneously. Different compressive strength values have been reported up to now for ECC, which are ranged from 10 MPa (designed for water fire-proofing) (25) to 200 MPa (High Strength ECC) (24).

For the 3D-printing of civil infrastructure, the implementation of fiber-reinforced ECC can yield significant benefits such as an enhanced structural capacity, durability, and resiliency. As such, ECC's unique mechanical properties place this novel composite as an excellent candidate for the 3D printing of concrete structures. While ECC is a promising material for 3D-printing implementation, several challenges still exist for its successful implementation (Marchon et al. 2018, Li et al. 2020a). To retain the ECC's strain-hardening property, high fiber content (~2% by volume) and small fiber diameter (typically below 50 μ m) are essential, leading to a paradoxical demand between pumpability and buildability (27).

Four crucial terms widely used in the determination of fresh properties of cementitious materials in the 3D-printing include flowability, extrudability, buildability, and open time (28). Flowability

is defined as the flow behavior of fresh material in a pumping system that guarantees the easy transportation of cement paste during pumping (29). The extrudability is the capability of fresh cement paste to pass through the nozzle as a continuous and intact filament (30) (31)(32). In addition, the buildability can be introduced as the bearing load capacity of printed filament to sustain their weight and weight of subsequent layers (Lim et al. 2012; (33); (12). It should be noted that the open time is defined as elapsed between the initial contact of dry mix and water and the time when the material is printable (flowable in the pumping system and extrudable in the printing (28). Previous research showed that a value between 19-25 cm for the flow table test in the first hour provides good flowability for the fresh concrete to pump and extrude 3D-printing concrete ink (34).

One of the green solutions to make concrete mixtures a more sustainable material is to partially substitute ordinary Portland cement (OPC) with supplementary cementitious materials such as fly ash and different types of slags (copper slag, steel slag), silica fume, and metakaolin. Previous studies (Curosu et al., 2016; Ding et al., 2018; Lei and Guo, 2018) showed the effect of incorporating these mineral admixtures in ECC's fresh and hardened properties and, accordingly, the printability characteristics of this material. It was indicated that the inclusion of silica fume between 5% to 10% weight of binder improves buildability and viscosity of the fresh 3D-printed mixture (38, 39). The optimum amount of silica fume can improve the flowability and cohesiveness of the mixture beyond which further addition of silica fume would cause a reduction in strength (40). Nano-clay (NC) has a considerable impact on cohesion and thixotropy of mixture and enhances the shape stability of the fresh 3D-printed mixture (Soltan and Li 2018, Bao et al. 2019, Zhu et al. 2019). A high content of NC exhibits low cohesion resulting in discontinuities in printing ink; on the other hand, the inclusion of 1 mass% NC enhances the compressive strength of specimen around 23 MPa in one day (43). Due to the spherical shape of the fly ash particles, the flowability of mixtures would improve; additionally, a lower surface area to volume ratio reduces water demand (44). It was shown that the high content of fly ash on ECC reduced the crack width due to the high interface frictional bond that restrains the slippage of fibers (Yang et al., 2007). Moreover, it was indicated that replacing cement with a high volume of fly ash (62% and 75% cement replacement with fly ash) resulted in tensile strength reduction but an increase in tensile ductility of ECC composites (46).

One of the major concerns in 3D printing of concrete is incompatibility of the conventional reinforcing techniques. The reinforcing bars utilized in normal construction practices can slow down the printing process and also reduce the degree of automation involved in this technology. Several researches and 3D printing companies have proposed different reinforcing methods such as pre-install reinforcement, in-process mesh reinforcement, post installation cages and prestress reinforcement (31, 47–49). However, in-effectiveness of these methods urges the researchers to look deeply into this matter. Although, 3D printable ECC could be another solution to the problem of the reinforcement in 3D printed concrete as it has potential to enhance the ductility and hence minimizing the requirement of conventional reinforcing bars. But, designing a 3D printable ECC is another challenge as the printing of ECC involved many issues including nozzle blockage, dispersion of fibers, poor surface quality, inconsistent dimensions and also insufficient buildability. This issue can be addressed by tailoring the rheological properties by incorporating some rheology modifiers. Viscosity modifying admixtures and some supplementary cementitious materials could be the appropriate choice in this case as suggested by some researchers (12, 42).

4. METHODOLOGY

4.1. Material and Mix Design

The primary objective of this study is to design a printable ECC with available materials from the local suppliers in region 6. To achieve this goal, we tried to contact the locals and prepare the required admixtures and materials for this study. The mineral/chemical admixtures and other constituents of ECC mixtures include (1) Type I/II Ordinary Portland Cement (C), (2) Type-F Fly Ash (FA), (3) River Sand (RS) with fineness modulus of 2.3 and a maximum size of 3.36, (4) High Range Water Reducer (HRWR), (5) Silica Fume (SF), (6) Iron Blast Furnace Slag (S), (7) Methyl Cellulose (MC), (8) non-oil coated RECS15 polyvinyl alcohol PVA fibers. Table 1 presents the chemical compositions of solid materials. The aggregate used in this study was natural river sand with a bulk dry specific gravity of 2.59 and an absorption capacity of 0.44%. Figure 1 displays the gradation curve of RS.

Table 1. Chemical composition of cementitious dry powders

Material	SiO ₂	Al ₂ O ₃	Fe ₂ O ₃	CaO	MgO	SO ₃	K ₂ O	TiO ₂	Na ₂ O	Specific Gravity
Cement (C)	19.24	4.75	3.35	65.8	2.20	3.61	0.54	0.21	-	3.13
Slag (S)	30.8	11.45	2.26	47.5	3.65	3.03	0.38	-	0.17	2.91
Silica fume (SF)	97.8	-	-	-	-	0.3	-	-	0.001	2.2
Fly Ash (FA)	61.27	23.18	5.09	2.11	1.19	0.30	1.43	-	1.44	2.09

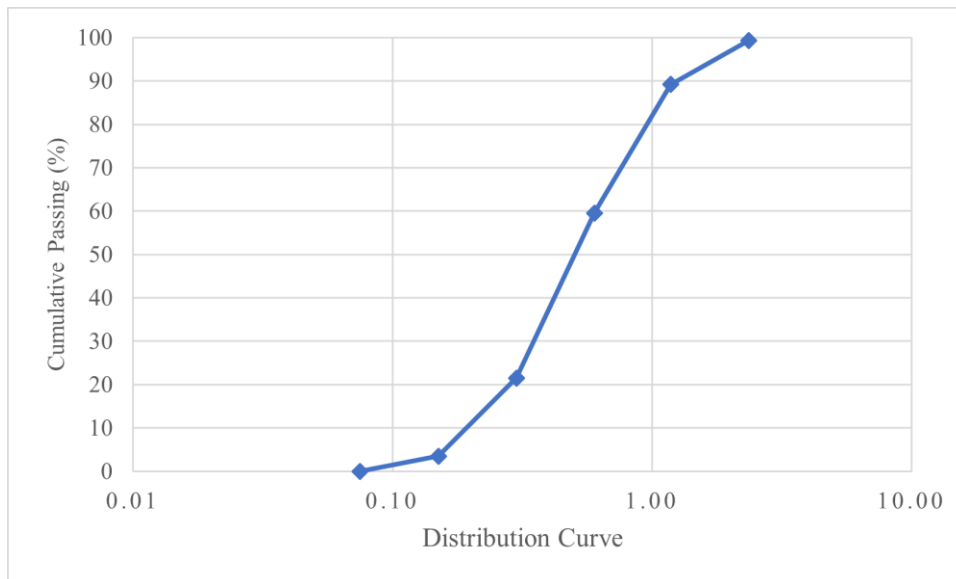


Figure 1. Particle size distribution (Gradation) of River Sand

In the preliminary phase of this study, 21 mixtures were designed and tested for setting time and compressive strength. Their list is presented in Table 2 for the two cement replacement levels (i.e., Cement/ Binder=0.25, 0.50). Different supplementary cementitious materials (i.e., FA, S, MK, SF) or their combination were used to form binary, ternary, and quaternary cementitious blends for each level. The focus of this study was mostly on fly ash replacement, and because of that, the Fly Ash/Binder ratios were evaluated at 0, 0.25, 0.40, 0.50, 0.65, 0.75. Then the slag substitution was studied for Slag/Binder: 0, 0.50, 0.75, and finally Silica Fume, Metakaolin and Methylcellulose were added as a rheology modifier according to the preliminary observation of the printing tests with lower content (i.e., Silica Fume /Binder: 0.0, 0.10, and Metakaolin /Binder ratios: 0.0, 0.10). The content of aggregate and High range water reducer was evaluated according to different experiments with different levels of fly ash, and for the rest of this study, they were kept constant at Aggregate/Binder=0.25, and HRWR/Binder=0.006.

Table 2. Mix design of different ECC mixtures

#	Mix ID	C/B	FA/B	S/B	SF/B	MK/B	W/B	RS/B	HRWR (%) ¹	Fibers (Vol%)
1	FA50- RS36- 0.30%	0.50	0.50	0.36	0.00	0.00	0.27	0.36	0.003	1.50
2	FA50-0.60%	0.50	0.50	0.00	0.00	0.00	0.27	0.25	0.006	1.50
3	FA50-MC-0.60%	0.50	0.50	0.00	0.00	0.00	0.27	0.25	0.006	1.50
4	FA65- RS39- 0.30%	0.35	0.65	0.00	0.00	0.00	0.27	0.39	0.003	1.50
5	FA75- RS36- 0.13%	0.25	0.75	0.00	0.00	0.00	0.27	0.36	1.3E-03	1.50
6	FA75- RS36- 0.30%	0.25	0.75	0.00	0.00	0.00	0.27	0.36	0.003	1.50
7	FA75- RS36- 0.40%	0.25	0.75	0.00	0.00	0.00	0.27	0.36	0.004	1.50
8	FA75-0.60%	0.25	0.75	0.00	0.00	0.00	0.27	0.25	0.006	1.50
9	FA50- 0.30%	0.50	0.50	0.25	0.00	0.00	0.27	0.25	0.003	1.50
10	FA65- 0.30%	0.50	0.65	0.25	0.00	0.00	0.27	0.25	0.003	1.50
11	S50-0.60%	0.50	0.00	0.50	0.00	0.00	0.27	0.25	0.006	1.50
12	S50-MC-0.60%	0.50	0.00	0.50	0.00	0.00	0.27	0.25	0.006	1.50
13	S75-0.60%	0.25	0.00	0.75	0.00	0.00	0.27	0.25	0.006	1.50
14	FA25-S50-0.60%	0.25	0.25	0.50	0.00	0.00	0.27	0.25	0.006	1.50
15	FA50-S25-0.60%	0.25	0.50	0.25	0.00	0.00	0.27	0.25	0.006	1.50
16	FA40-SF10-0.60%	0.50	0.40	0.00	0.10	0.00	0.27	0.25	0.006	1.50
17	FA40-SF10-MC-0.60%	0.50	0.40	0.00	0.10	0.00	0.27	0.25	0.006	1.50
18	FA40-MK10-0.60%	0.50	0.40	0.00	0.00	0.10	0.27	0.25	0.006	1.50
19	FA40-MK10-MC-0.60%	0.50	0.40	0.00	0.00	0.10	0.27	0.25	0.006	1.50
20	FA65-SF10-0.60%	0.25	0.65	0.00	0.10	0.00	0.27	0.25	0.006	1.50
21	FA40-S25-SF10-0.60%	0.25	0.40	0.25	0.10	0.00	0.27	0.25	0.006	1.50

Note: 1. %HRWR dosage by weight of Binder

2. C: Cement; FA: Fly Ash; S: Slag; MK: Metakaolin; SF: Silica Fume; W: Water; RS: River Sand; B: Binder; HRWR: High Range Water Reducer, MC: MethylCellulose

3. all ratios are weight (wt) ratio but the volumetric fiber content.

According to the preliminary phase of the study in Fall 2020, the UNM team noticed that when the level of cement replacement is 0.75, it was hard to achieve acceptable mechanical and printability performance. Thus, eight of ECC mixtures were selected and tested for the rest of this study (Table 2). The mixtures were highlighted in yellow in Table 2 and labeled according to the weight (wt) percentages of additives and viscosity modifier as FA50 (representing a hybrid binder of 50% (wt) FA and 50% (wt) C); FA50-MC (representing a hybrid binder of 50% (wt) FA, 50% (wt) C and 1% (wt) of total weight MC), S50 (representing a hybrid binder of 50% (wt) S and 50% (wt)

C), S50-MC (representing a hybrid binder of 50%(wt) S, 50%(wt) C and 1%(wt) of total weight MC), FA40-SF10 (representing a hybrid binder of 40%(wt) FA, 10%(wt) SF and 50%(wt) C), FA40-SF10-MC (representing a hybrid binder of 40%(wt) FA, 10%(wt) SF, 50%(wt) C and 1%(wt) of total weight MC), FA40-MK10 (representing a hybrid binder of 40%(wt) FA, 10%(wt) MK and 50%(wt) C) and FA40-MK10-MC (representing a hybrid binder of 40%(wt) FA, 10%(wt) MK, 50%(wt) C and 1%(wt) of total weight MC).

4.2. Mixing Procedure and Test Methods

To ensure consistency of the mixture, preparation and mixing of the ECC mortars followed a specific procedure. All mortars were mixed following ASTM C305-14. Dry powders, i.e., cement, fly ash, slag, silica fume, and river sand) were drily mixed in advance and consistently for 15 min at slow speed (140 ± 5 RPM) in a Hobart mixer. HRWR dissolved in water, then added to the dry powders slowly and mixed with them for another 5 minutes. Finally, PVA fibers were added to the mixture and blended with other ingredients for 10 minutes at medium speed (285 ± 10 RPM).

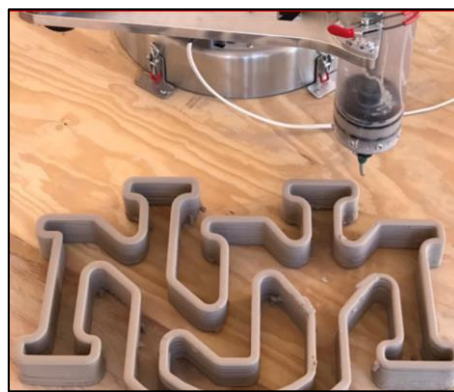
The baseline of this study is checking the mechanical and fresh properties of the ECC mixtures based on their flowability. For evaluating the mechanical properties of designed ECCs, the characteristics such as compressive strength, flowability, and setting time were assessed. This procedure paved the way to reach a mix-design appropriate for 3D printing. The details of how the tests were performed are presented in this section.

4.3. 3D-Printing System

A gantry 3D-printing system from the new Dana C. Wood Materials and Structures Lab at UNM will be utilized for the manufacturing of these specimens (Figure 2). The hardened properties of 3D-printed specimens will be evaluated and compared to those of traditionally cast-in-place ECC specimens. The large-scale printer (Figure 2a) is a cartesian coordinate robot system with three linear translational degrees of freedom and 0 rotational degrees of freedom. This means the three principal axes of control are linear (i.e., they move in a straight line rather than rotate) and are at right angles to each other (51). This robotic configuration is highly reliable, precise, and robust while operating in a 3-dimensional space. This type of robot is widely used for 3D printing. The printer is placed on the floor, which is also the building platform. The specifications of this printer are shown in the Appendix.



(a)



(b)

Figure 2. UNM Dana C. Wood Materials and Structures Lab 3D-Printing Systems (a) 3D-Printing of Concrete (b) 3D-Printing of Clay

4.4. Pretests

In the light of the flow-characteristic influence on the printability of the fresh ECC mixtures, in this part of the research, the attempt was made to develop different ECC mixtures by fixing the flow table of fresh mixtures in the range 19-20 cm. For all mixtures, the Water to Binder (including a combination of C, FA, S, and SF) ratio, (W/B) wt, was maintained at 0.27; the quantity of HRWR was 150 ml per 100 kg of the cementitious binder. After mixing the materials, the flow table test was conducted, and the amount of water for each mixture was adjusted (water was either added or removed) to achieve 19-20 cm flow table test results.

4.4.1. Setting time test

The initial setting time is defined as the time elapsed from the first contact of dry mix powder with water until the paste is stiffened enough to reach a penetration resistance of 3.5MPa. (ASTM C125 - 20) Open time is a new term that is mostly used for the 3D-printing, and it is defined as the time elapsed between the instant of adding water until the time that fresh paste is printable (53). Previous studies (Kazemian et al. 2017, Panda et al. 2019) indicated that the open time of printable concrete is always before the initial setting time. While there is no direct relation between setting time and open time for printable concrete, it can be assumed that the longer initial setting time results in a longer open time. In this study, we are using this test method as an indirect indicator for the open time. The convenient test method that gives the researcher the progress of structuration over time is the Vicat needle test (i.e., ASTM C191 -19) and shown in **Error! Reference source not found.** To perform this test method, the fresh cement paste is molded in a container (measuring 70mm top opening diameter by 80mm bottom opening diameter in 40mm height), and a periodic test is done to outline the setting status. In this test, a straight steel needle is used to penetrate the cement paste in the mold. The penetration shows the trend of setting procedure; the more is the needle penetration; the lower is the stiffness of cement paste. The penetration is a way to indicate the initial setting time, when the Vicat test is continued until penetration value reaches 25mm. Before this point, due to the softness of the cement paste, the penetration depth is greater. The final setting time, according to this method, is the time elapsed from the first contact of water and dry ingredient and time at which the 1-mm needle does not leave any complete circular impression on the surface of cement paste. For the final setting time, two additional points on different sides of the cement paste were tested.



Figure 3. Vicat needle test

4.4.2. Flow table test

The fresh behavior of cementitious materials plays an essential role in the flowability and extrudability of the mixtures for the 3D-printing. The more flowable the cementitious mixture, the easier movement and extrusion of fresh material occur in the hose/extruder for the 3D printing process. The flowability of the specimens was evaluated according to ASTM C1437 - 15 and shown in **Error! Reference source not found.** In this test, after placing the conical mold (70mm top diameter by 100mm bottom diameter in 50mm height) at the center of the standard flow table, one layer of mortar of about 25mm of thickness was added into the mold and tamped 20 times. Subsequently, the mold was filled with the second layer and tamped 20 times. To make a plane surface even surface, the extra mortar was removed. The cone-shape mold was lifted, and the top table and remained mortar system is shaken by dropping the table 25 times per 15s. The diameter of mortar on the table surface should be recorded just before and after the table dropping. The flow table results of different mixtures were kept constant between 19-20 mm by adjusting the W/B ratio to have a flowable mortar for the printing process.



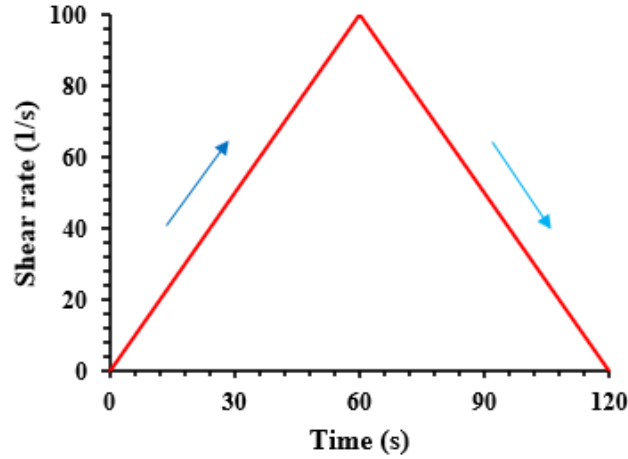
Figure 4. Flow table test

4.5. Rheology

A Brookfield Rheometer RST-SST was used for rheological measurements of ECC mixtures equipment with a vane spindle of designation VT20-40 (diameter = 20 mm and length = 40 mm) shown in figure 5 (a). The range of shear stress provided by the manufacturer for this vane spindle is 5.2 Pa to 3.4 KPa. The protocol used for the rheology measurements is the hysteresis technique adopted from the literature (57) shown in Figure 5 (b). The hysteresis technique quantifies the static yield stress as it does not have any pre-shearing zone. The total testing time was 120 seconds; during the first 60 s the shear rate was ramped up from 0 s⁻¹ to 100 s⁻¹ and again ramped down from 100 s⁻¹ to 0 s⁻¹ in the last 60 seconds. In addition, the plastic viscosity, yield stress, and thixotropy of ECC mix by adopting the Bingham model as shown in Fig 6 were calculated by measuring the shaded area between the shear rate of 20 s⁻¹ and 80 (34, 58). Total three trials were performed for each mix, and an average of these results was reported. All the measurements were taken in a controlled temperature and humidity conditions.



(a)



(b)

Figure 5. (a) Brookfield Rheometer RST-SST (b) Hysteresis loop testing profile

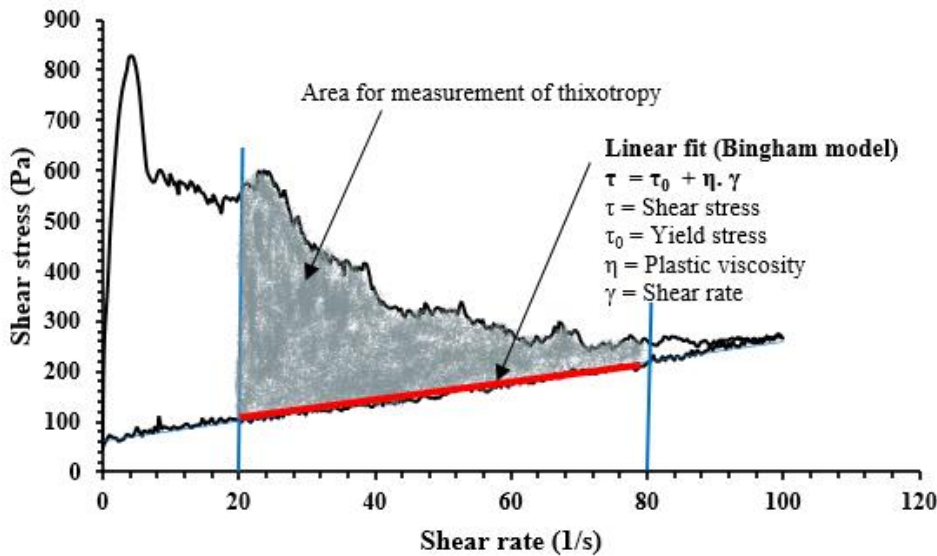


Figure 6. The experimental approach to measuring plastic viscosity, yield stress, and thixotropy adopts the Bingham model.

4.6. 3D-printing Tests

The printability of ECC mixtures was evaluated in terms of extrudability and buildability. Since the printing quality of ECC mixtures wasn't satisfying, MC was introduced as a viscosity modifying admixture to improve the printing quality. The printing took place in a controlled room with a constant temperature of 23 ± 2 °C.

4.6.1. Extrudability

Extrudability is necessary to ensure the printing of intact filament of desired width and thickness. The printing system mainly governs it in terms of printing and extrusion speeds. To evaluate this,

60 × 60 cm hollow squares were printed (shown in 7) with different printing and extrusion speeds. The printing speed was kept constant as 1, 2, 4, and 5 cm/s, while the extrusion speeds were adjusted for each ECC mixture. After 24 hours, the width and thickness of each side of squares at five different locations and all the corners were measured to evaluate the printing quality in terms of dimension conformity and consistency. The average values were reported to compare the printing quality of standard ECC mixtures and the mixtures with the addition of MC. Moreover, the effect of different extrusion and printing speeds on the quality of printing is also analyzed.

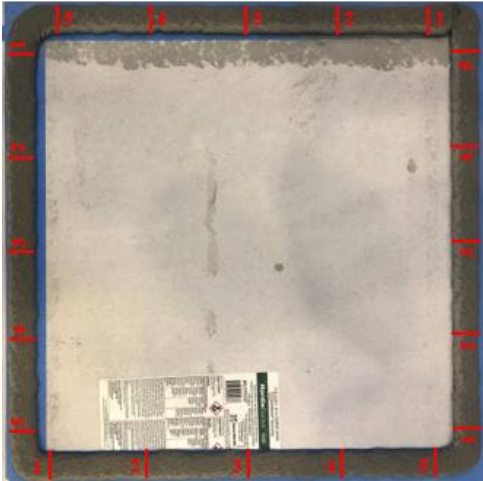
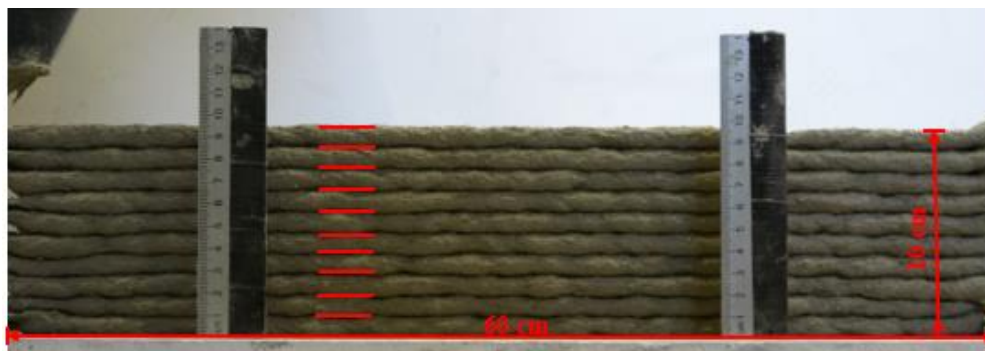


Figure 7. 60 x 60 cm 3D-printed hollow square for the extrudability evaluation

4.6.2. Buildability

Buildability is the material's ability to retain the extruded shape of the filament against its load and a load of filaments deposited above it by limiting the deformations. To evaluate the buildability, single-layered walls stacked with ten layers of 1 cm thickness were printed, as shown in 8. The total height of the wall was measured and compared with the designed height of the wall, which was 10 cm. Furthermore, the thickness of the bottom layer was recorded after printing each layer to monitor the deformation of the bottom layer due to a load of subsequent layers. To evaluate the deformation of the mixtures, the printing time interval between each layer was evaluated in 0 and 5 minutes. The printing speed and extrusion speed were adopted from the extrudability trial results of each mixture based on the better printing quality.



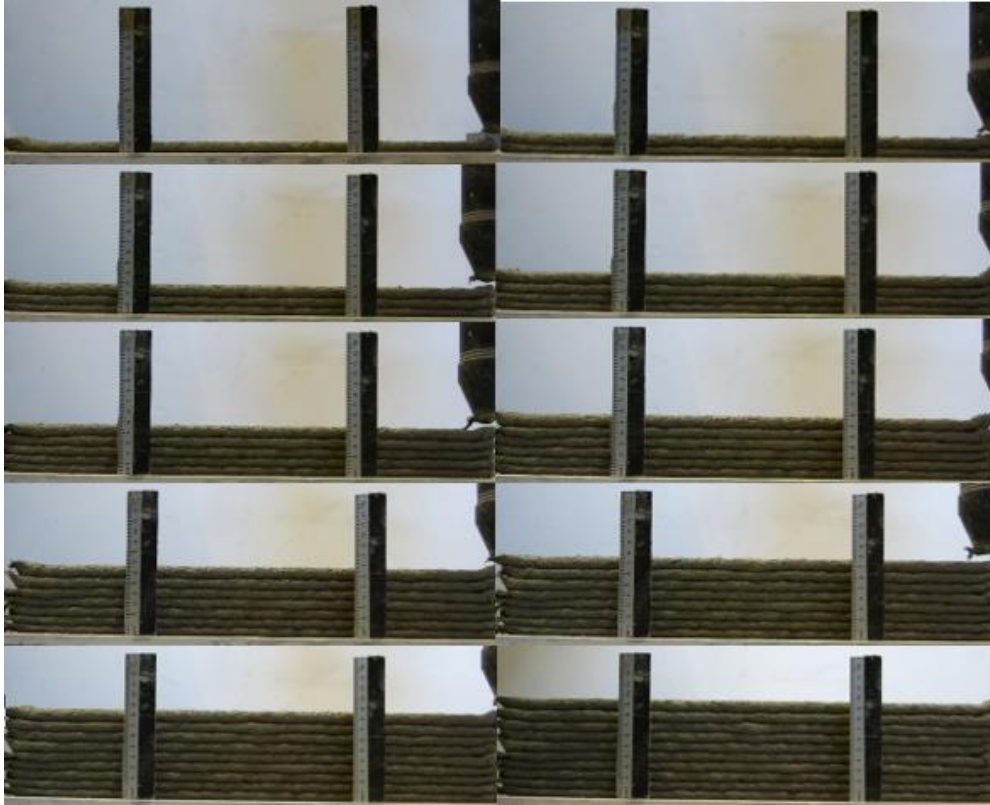


Figure 8. 3D-printed wall for the buildability evaluation

4.7. Mechanical Properties

4.7.1. Compressive strength test (Cast Specimens)

The compressive strength of the designed ECCs indicates the suitability of these materials for structural applications. Therefore, it is worthy of studying the viability of prepared mixtures by assessing their compressive strength. To measure the compressive strength of mixtures, the fresh mortar was cast in two layers of $50 \times 50 \times 50$ mm cube molds immediately after mixing according to ASTM C109-20. Each layer of mortar was compacted 25 times with a rod. The samples were demolded at 24 hours and then moist cured (100% RH, $23 \pm 0.5^\circ\text{C}$) until the testing day. The cubes were tested after 7, 14 days and 28 days at a loading rate of 0.25 MPa/s.

4.7.2. Direct tension test

A Bionix servo-hydraulic testing machine was employed to conduct the uniaxial direct tension test on dog-bone specimens. The displacement rate of 0.5 mm/min has been chosen following the recommendation of the Japan Society of Civil Engineers (JSCE). For each mixture containing MC, three dog-bone specimens have been cast. After casting, specimens were adequately treated by covering their top with a plastic sheet until the demolding day. Then, the samples were transferred into the moisture room (100% RH, $23 \pm 0.5^\circ\text{C}$) and cured till the testing day. Fig. 9. illustrates the test setup and the prepared samples, two linear variable displacement transducers (LVDTs) were mounted to the dog-bone specimens to measure the elongation of the gauge length after applying the load.

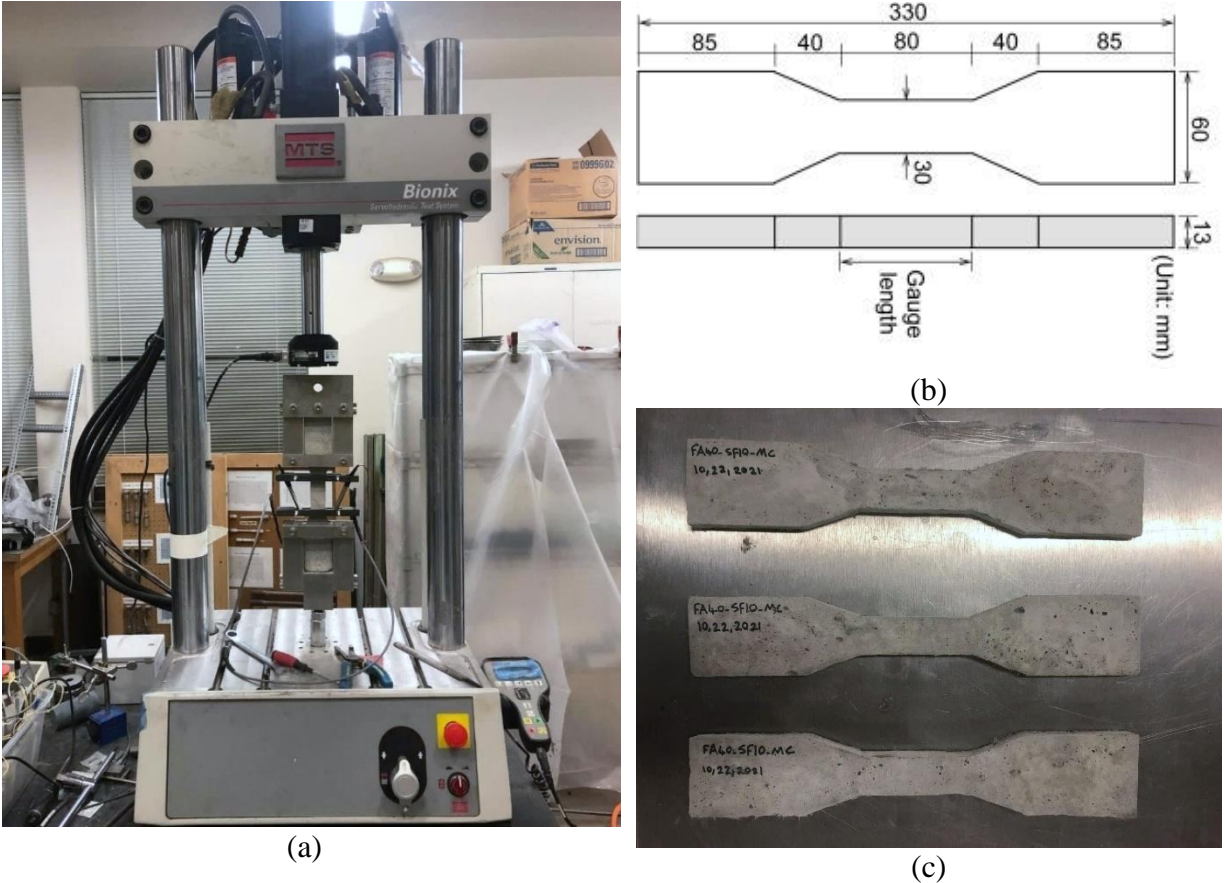


Figure 9. (a) Uniaxial direct tension test setup, (b) specimens dimension according to JSCE recommendations, (c) casted dog-bone sample

4.7.3. Compressive strength tests (Printed Specimens)

For the printed specimens created from each mixture, a primary prism sample consists of six layers in 150×150 mm and a total height of 60 mm printed using the gantry system. After 24 hours, the samples were moist cured (100% RH, $23 \pm 0.5^\circ\text{C}$) until the testing day. Four small cubes of $50 \times 50 \times 50$ were extracted from the primary cubic sample using a wet tile saw during testing day. All specimens were tested perpendicular to the printing direction. The cubes were tested after 28 days at a loading rate of 0.25 MPa/s according to ASTM C109-20. Fig 10 displays the 3D-printed cubes prepared for the compressive strength tests.

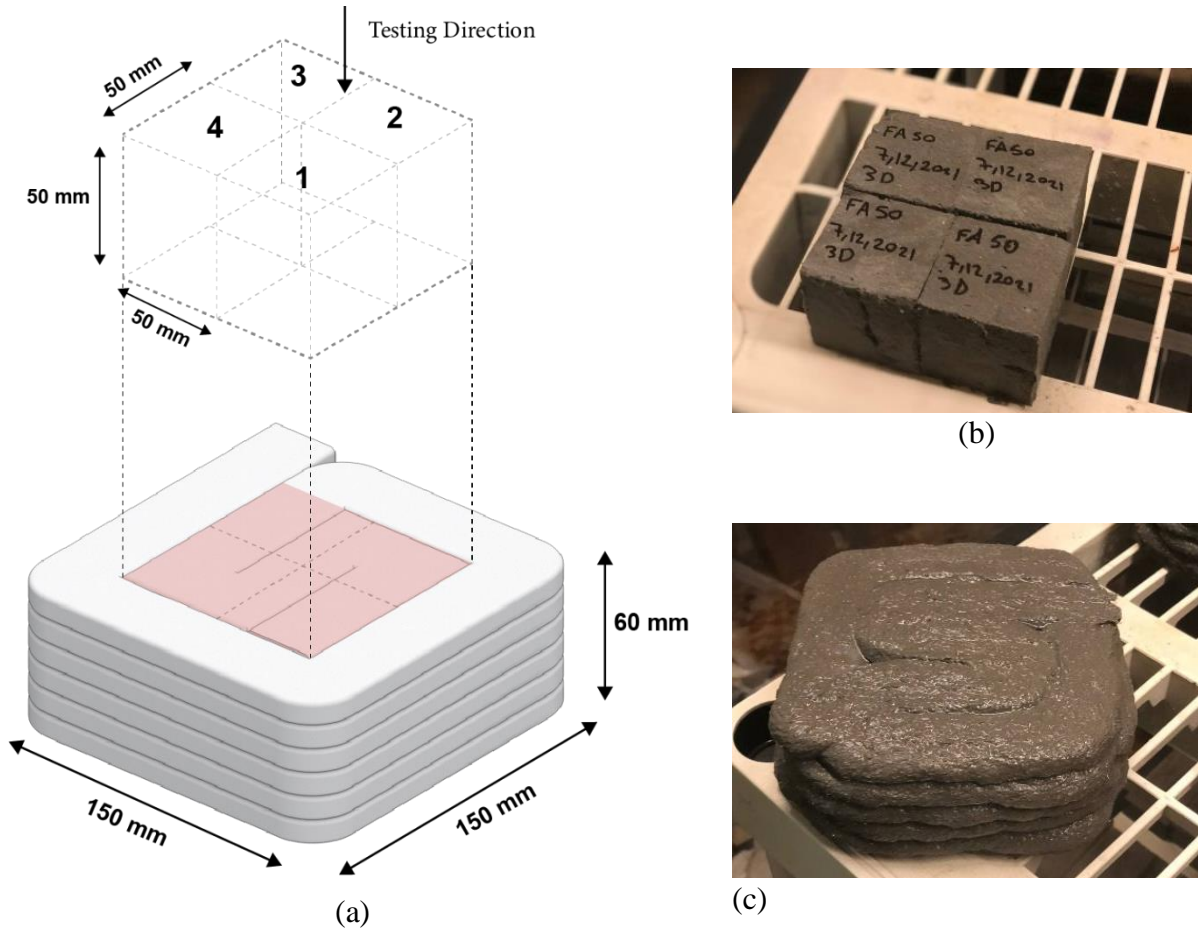
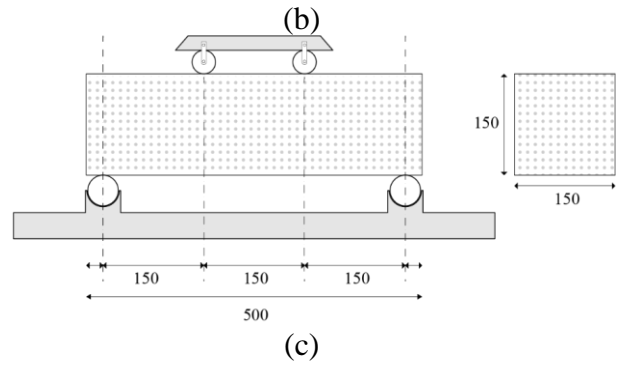


Figure 10. (a) Testing direction and cutting diagram of four cubic samples extracted from 150×150×60mm primary prism sample, (b) primary prism sample, (c) four extracted 50×50×50mm cubic samples from the primary sample.

4.7.4. Beam tests (3D Printed)

This research also evaluates the flexural behavior of ECC 3D-printed beams. Three rectangular specimens made of FA40-SF10-MC having the dimension of 100×100×500 mm in 10 layers have been printed using the gantry system with the 20 mm diameter circular nozzle. The specimens were transferred to the moisture room and cured (100% RH, 23±0.5°C) till the testing day (28-days after printing). The printed beams will be subjected to pure bending; a three-point flexural test according to the ASTM C1609-19 has been conducted on the specimens using a hydraulic Universal testing system. The load rate applied to the specimens is 0.075 mm/min. The applied load will be recorded on a recording systems software during the three-point bending test. Additionally, the machine automatically records the deflection of the ECC specimens by LVDT's connected to the Universal testing machine. Fig 11 displays the testing machine and 3D-printed specimen.



(a)

(b)

(c)

Figure 11. (a) Three-point bending test setup, (b) 3D-Printed beam, (c) designed beam using 3D software

5. ANALYSIS AND FINDINGS

5.1. Fresh Properties

5.1.1. Flow Table Test Results

Since designed ECC mixtures exhibited different water demands in their fresh stage, and to keep them all flowable and buildable for the 3D-printing phase, we decided to adjust the water to binder ratio according to the flow table results in this preliminary stage of the study. Table 9 displays the amount of flow table test results of different mixtures. The amount of adjusted water to binder (W/B) ratio in Table 3 indicates that the fly ash-rich ECC mixtures led to a lower adjusted W/B ratio (i.e., 0.26) than those of other mixtures. It is likely that the spherical shape of fly ash particles makes them act as a lubricant in the fresh ECC mixtures; thus, they need a lower amount of water to reach a specific flow. In contrast, the ECC mixtures contain a large slag; they need more water to get a 19-20 cm flow table (i.e., adjusted W/B=0.33).

Moreover, the mixtures containing MC have quite different flow behavior as compared to the standard mixtures. The W/B ratios were adjusted for the MC-rich mixtures to get better printability. A contrasting behavior was observed, which questioned the reliability of the flow table results with the addition of MC.

Table 3. Flow table results of standard ECC mixtures.

#	Mix ID	Flow Table (mm)	Initial W/B	Adjusted W/B
1	FA50	20	0.27	0.26
2	S50	19.8	0.27	0.33
3	FA40-SF10	19	0.27	0.33
4	FA40-MK10	20	0.27	0.3

Table 4. Flow table results of ECC mixtures containing MC.

#	Mix ID	Flow Table (mm)	W/B
1	FA50-MC	13.5	0.23
2	S50-MC	15.5	0.30
3	FA40-SF10-MC	14.7	0.27
4	FA40-MK10-MC	14.5	0.27

5.1.2. Rheology

The rheological properties of ECC mixtures: FA50, FA40-SF10, FA40-MK10, S50, FA50-MC, FA40-SF10-MC, FA40-MK10-MC and S50-MC are presented in Fig 14 to Fig 21. The rheological evolution over time was studied for the age of 0, 15, 30, 45, and 60 minutes. The rheological parameters such as plastic viscosity, static yield stress, dynamic yield stress, and thixotropy were significantly increased with the addition of MC as compared to the standard ECC mixtures without MC. This effect can be attributed to the potential of MC to retain the water and increase the viscosity and thixotropy (42). Moreover, MC can bridge the cement particle by adsorbing on their surface, which leads to the improvement of macroscopic yield stress (60). Fig 12 and Fig 13 depict

the shear stress vs. shear rate curves and linear fits between the shear rate of 20 s⁻¹ and 80 s⁻¹ of ECC mixtures, respectively.

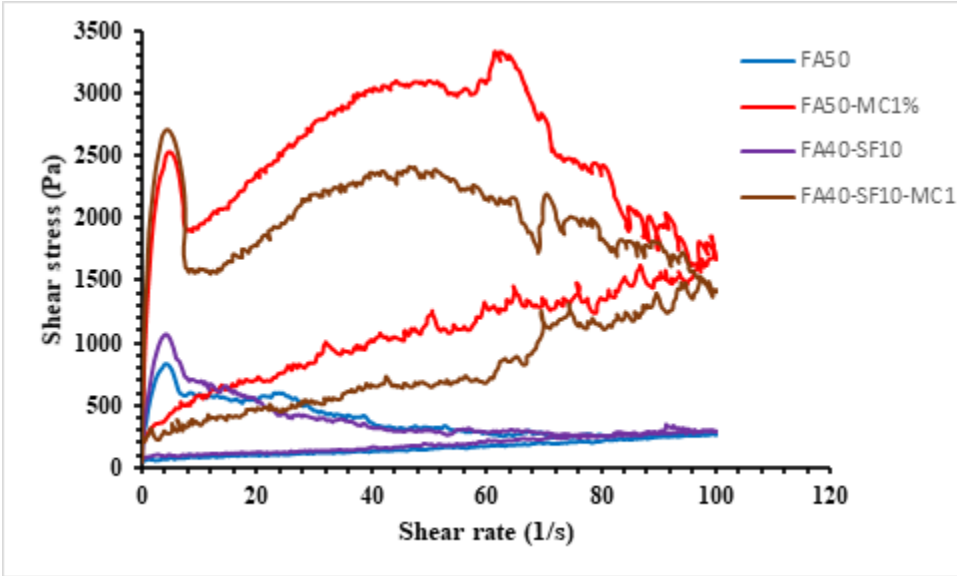


Figure 12. Hysteresis curves of ECC mixtures.

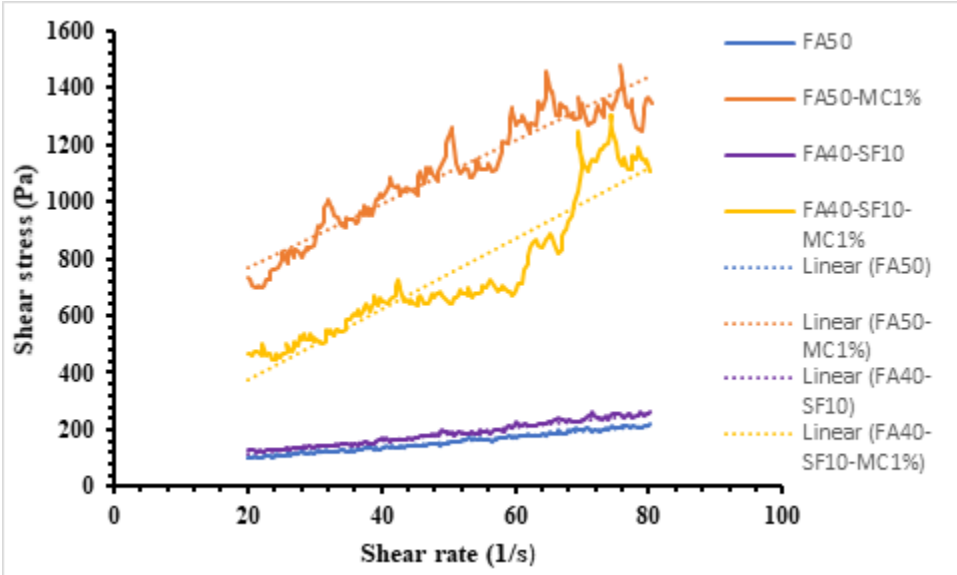


Figure 13. Plastic viscosity and yield stress of ECC mixtures (Linear fits are used to measure)

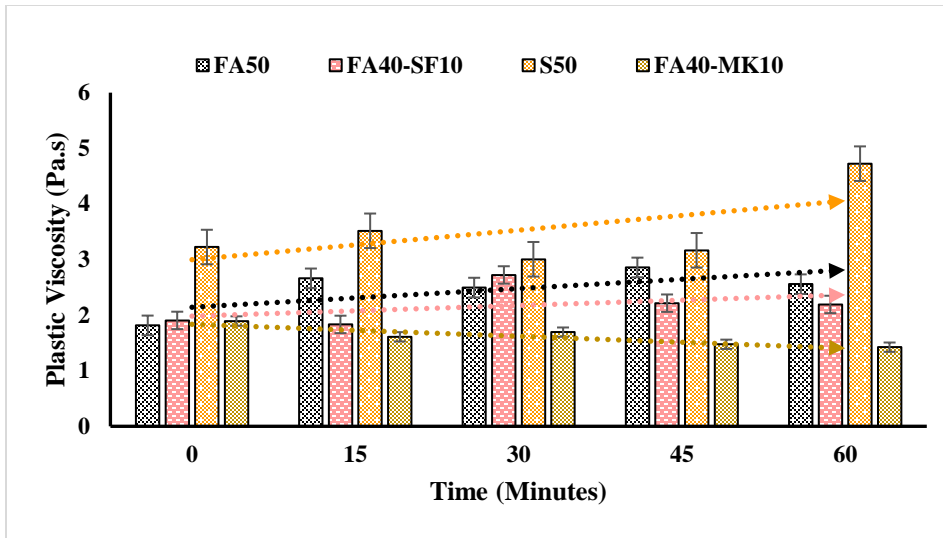


Figure 14. Plastic Viscosity of standard ECC mixes

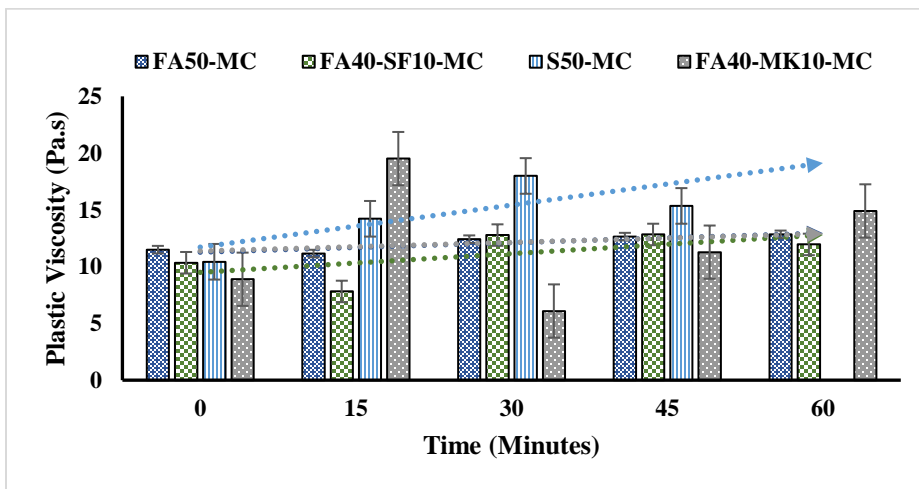


Figure 15. Plastic Viscosity of ECC mixes with MC

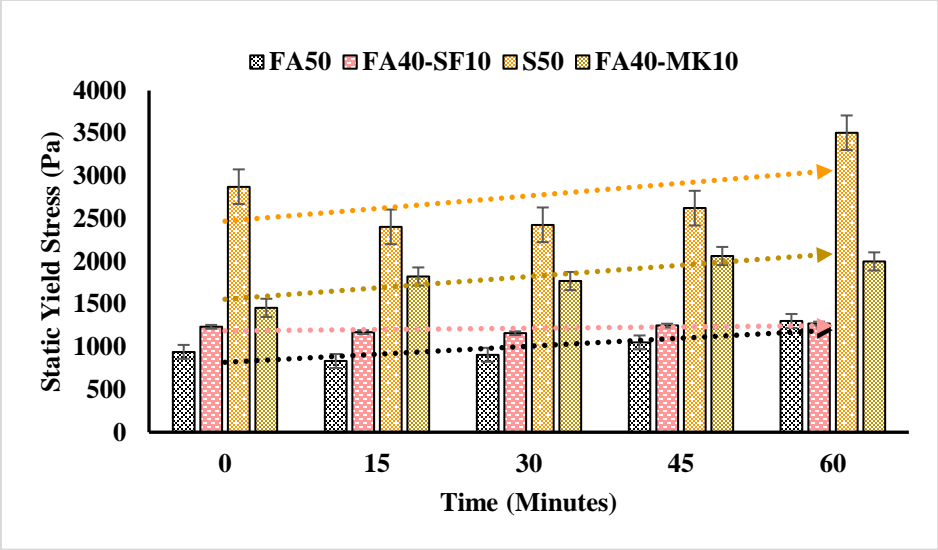


Figure 16. Static Yield Stress of standard ECC mixes

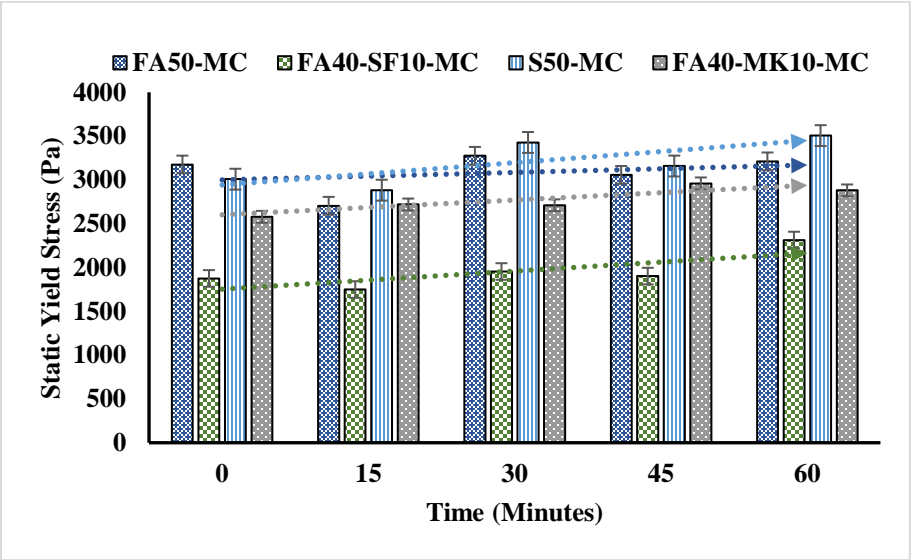


Figure 17. Static Yield Stress of ECC mixes with MC

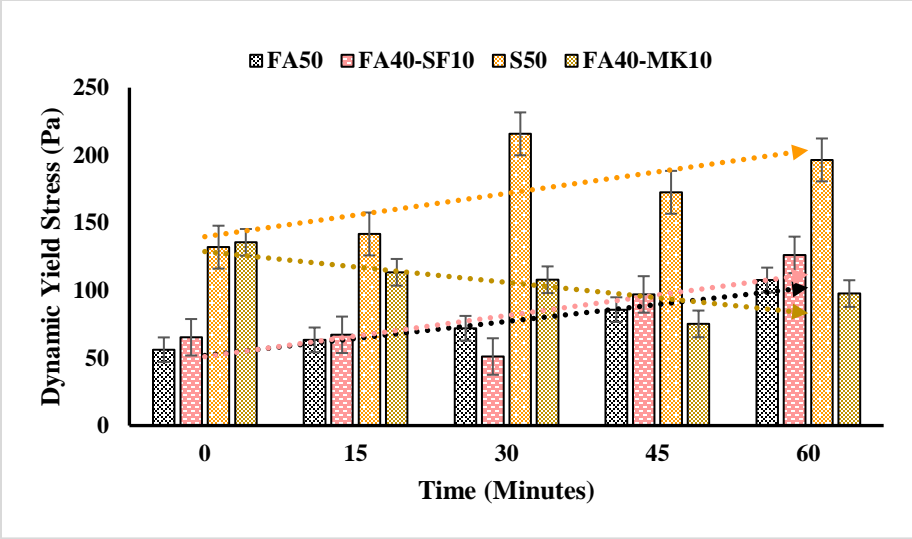


Figure 18. Dynamic Yield Stress of standard ECC mixes

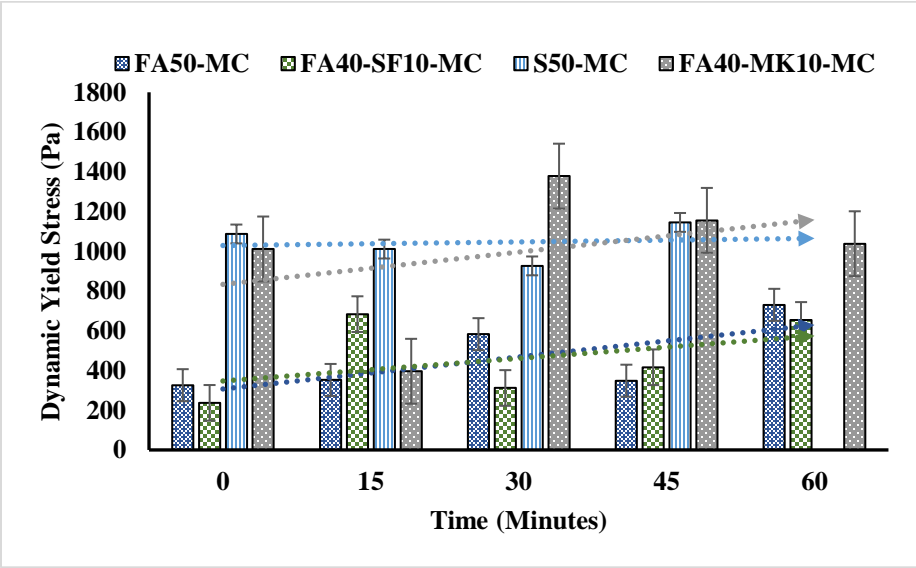


Figure 19. Dynamic Yield Stress of ECC mixes with MC

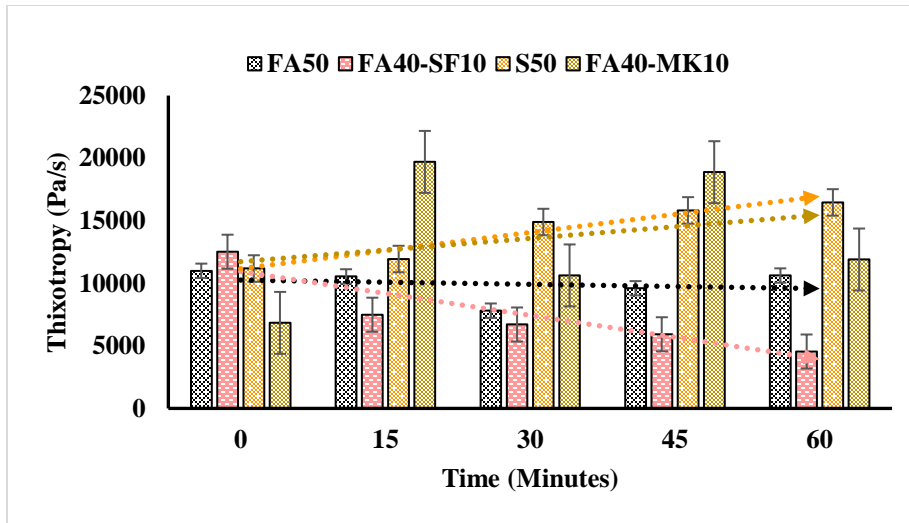


Figure 20. Thixotropy of standard ECC mixes

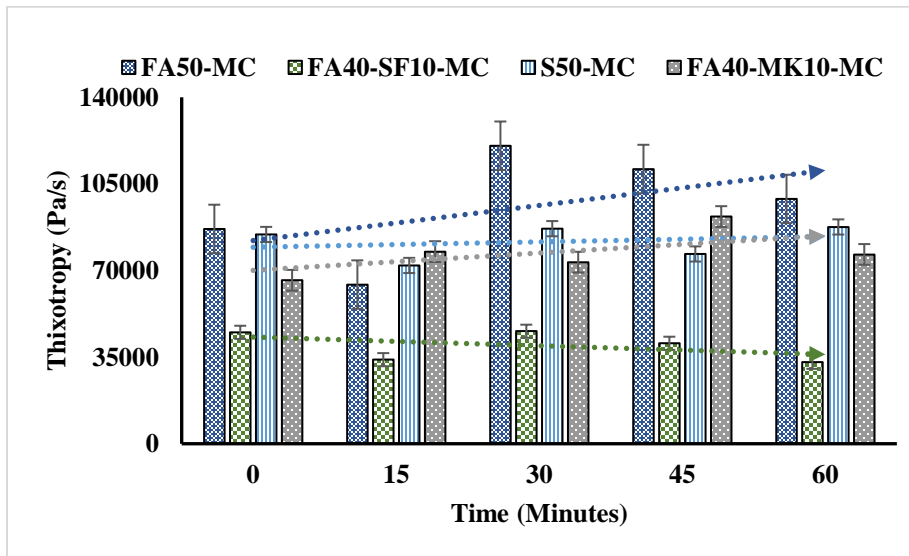


Figure 21. Thixotropy of ECC mixes with MC

5.2. Printability

5.2.1. Extrudability

The extrudability tests were performed to evaluate the printing quality of ECC mixtures in terms of dimension conformity and consistency of the printed layers; also, the corners of the printed layers are analyzed. The results of all the ECC mixtures with and without the addition of MC are reported from **Error! Reference source not found.** to **Error! Reference source not found.** for different printing speeds. The average width, average thickness, and the standard deviation of all the printed squares are presented. The results represent that the printing quality was significantly improved with MC incorporation. The dimensions conformity and consistency were marginally

improved for the mixtures with MC. During the mixing process, the fibers clustering phenomena were observed, which mitigated the uniform dispersion of the fibers in the mix. The printed filament was not intact due to the fiber clustering, which influenced the printing quality of the ECC mixtures without MC. However, the above said phenomena were not observed in the mixtures containing MC, which endorse the role of MC in promoting the better dispersion of the fibers. The better printing quality can be attributed to the better distribution of the fibers in the ECC mixtures with MC.

Furthermore, the printing speed and extrusion speed are other parameters that can affect extrudability. Although, the extrusion speed was different for each ECC mix because every mix has different ingredients and flow properties. However, the printing speed was kept constant as 1, 2, 4, and 5 cm/s for all the mixtures to observe the effect on the extrudability. During the printing trials, the printing speed of 4 cm/s was the best for most of the mixtures as it provided better printing quality.

Table 5. Extrudability evaluation results at 1 cm/s printing speed













Printing Speed = 1 cm/s					
Mix ID	Average Width (mm)	Standard Deviation (Width)	Average Thickness (mm)	Standard Deviation (Thickness)	Printing Quality
FA50-Standard	34.092	2.944	11.745	0.988	
FA50-MC (W/B 0.23)	31.676	1.0737	11.759	0.729	
FA50-MC (W/B 0.25)	33.853	1.561	11.71	0.626	
FA40-SF10 Standard	28.808	1.606	12.398	0.7887	
FA40-SF10-MC1 (W/B 0.27)	34.774	3.594	11.612	0.928	
FA40-SF10-MC1 (W/B 0.30)	30.164	1.645	10.618	0.739	
FA40-MK10 Standard	35.982	2.902	10.88	0.656	
FA40-MK10-MC (W/B 0.27)	26.197	1.9113	14.324	0.756	
FA40-MK10-MC (W/B 0.30)	35.286	1.869	10.697	0.512	
S50 Standard	30.293	5.045	9.248	0.8574	
S50-MC (W/B 0.27)	23.243	2.346	12.082	0.64	
S50-MC (W/B 0.30)	31.738	1.369	11.864	0.389	

Table 6. Extrudability evaluation results at 2 cm/s printing speed.

Printing Speed = 2 cm/s					
Mix ID	Average Width (mm)	Standard Deviation (Width)	Average Thickness (mm)	Standard Deviation (Thickness)	Printing Quality
FA50-Standard	34.01	2.593	11.949	0.7353	
FA50-MC (W/B 0.23)	30.39	1.055	11.823	0.684	
FA50-MC (W/B 0.25)	30.188	1.097	11.368	0.4892	
FA40-SF10 Standard	39.278	3.978	14.114	0.568	
FA40-SF10-MC (W/B 0.27)	35.556	1.709	11.907	1.0534	
FA40-SF10-MC (W/B 0.30)	27.095	1.354	10.255	0.693	
FA40-MK10 Standard	36.177	2.494	10.501	0.65	
FA40-MK10-MC (W/B 0.27)	23.774	1.913	12.394	0.863	
FA40-MK10-MC (W/B 0.30)	30.477	1.824	10.055	2.206	
S50 Standard	33.13	1.899	10.383	1.138	
S50-MC (W/B 0.27)	24.647	0.933	12.221	0.475	
S50-MC (W/B 0.30)	28.809	1.215	11.845	0.471	

Table 7. Extrudability evaluation results at 4 cm/s printing speed.






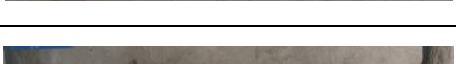
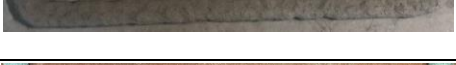



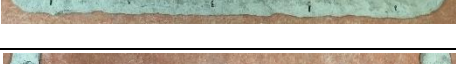




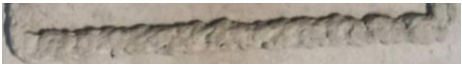






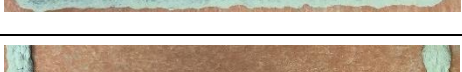

Printing Speed = 4 cm/s					
Mix ID	Average Width (mm)	Standard Deviation (Width)	Average Thickness (mm)	Standard Deviation (Thickness)	Printing Quality
FA50-Standard	30.353	3.602	11.742	0.809	
FA50-MC (W/B 0.23)	28.488	1.0068	11.439	0.793	
FA50-MC (W/B 0.25)	26.383	1.254	10.728	0.806	
FA40-SF10 Standard	28.435	1.558	13.483	0.814	
FA40-SF10-MC (W/B 0.27)	28.66	1.255	10.963	1.025	
FA40-SF10-MC (W/B 0.30)	29.297	1.703	10.365	0.69	
FA40-MK10 Standard	31.374	2.287	11.617	0.605	
FA40-MK10-MC (W/B 0.27)	24.881	1.72	12.344	0.463	
FA40-MK10-MC (W/B 0.30)	27.891	2.737	9.876	0.67	
S50 Standard	33.987	2.982	9.875	0.915	
S50-MC (W/B 0.27)	25.355	2.733	11.67	0.619	
S50-MC (W/B 0.30)	25.785	0.845	10.935	0.693	

Table 8. Extrudability evaluation results at 5 cm/s printing speed.

Printing Speed = 5 cm/s					
Mix ID	Average Width (mm)	Standard Deviation (Width)	Average Thickness (mm)	Standard Deviation (Thickness)	Printing Quality
FA50-Standard	31.088	1.951	11.056	0.875	
FA50-MC (W/B 0.23)	27.282	0.598	11.469	0.339	
FA50-MC (W/B 0.25)	27.633	0.989	11.5	0.591	
FA40-SF10 Standard	31.396	2.361	13.146	0.633	
FA40-SF10-MC (W/B 0.27)	24.011	1.538	11.172	0.757	
FA40-SF10-MC (W/B 0.30)	27.533	1.13	10.803	0.53	
FA40-MK10 Standard	32.235	1.936	11.068	0.426	
FA40-MK10-MC (W/B 0.27)	23.06	1.855	12.401	0.59	
FA40-MK10-MC (W/B 0.30)	24.369	1.54	10.56	3.088	
S50 Standard	31.833	2.005	10.049	0.811	
S50-MC (W/B 0.27)	22.852	1.471	12.185	0.484	
S50-MC (W/B 0.30)	26.949	0.908	11.163	0.608	

5.2.2. Buildability
















The buildability results of ECC mixtures are presented in Table-9. The designed height and length of the printed wall were 10 cm and 60 cm, respectively. The actual height of the printed wall and thickness of the bottom layer was observed to calculate the deformation of the bottom layer due to the load of the subsequent layers. The printing speed was selected as 4 cm/s to print the walls based on the results of the extrudability evaluation as this speed provided better printing quality. The buildability was assessed both for zero-time intervals between the layers and 5 minutes time intervals. A similar trend as extrudability was observed that the buildability was significantly improved with the addition of MC in the ECC mixtures. The total height of the printed object and thickness of the bottom layer was almost the same as the designed value showing negligible deformations in the printed filaments. This behavior can be attributed to the improved rheological properties, specifically yield stress and thixotropy due to MC addition. On the other hand, most of the mixtures without MC were either collapsed or were not extrudable at the zero-time interval. Although the ECC mixtures were printed with 5 minutes, the time gap between layers possesses decent shape retention, the interlayer bond between the printed filaments was disturbed, as shown in Fig 22.

Conclusively, the MC is an efficient viscosity modifying admixture in ECC mixtures as it has the potential to improve the printing quality in terms of dimension conformity, dimension consistency, surface quality, buildability, and shape retention.



Figure 22. Cross-sections of walls printed for buildability evaluation (left to right) (a) at 0 minutes time gap (b) at 5 minutes time gap

Table 9. Buildability evaluation of different ECC mixtures.

Mix #	Time Interval	First Layer Height (mm)	Total Height (mm)	Number of layers	Printed objects
FA40-SF10	0 Time interval	8	50	5	
	5 Time interval	9	100	10	
FA40-SF10-MC	0 Time interval	7.5	100	10	
	5 Time interval	8.5	100	10	
FA50	0 Time interval	5	60	6	
	5 Time interval	7	100	10	
FA50-MC	0 Time interval	7	100	10	
	5 Time interval	9	100	10	
FA40-MK10	0 Time interval	8.5	100	10	
	5 Time interval	8.5	80	8	
FA40-MK10-MC	0 Time interval	8	100	10	
	5 Time interval	9	100	10	
S50	0 Time interval	8	100	10	
	5 Time interval	8	50	5	
S50-MC	0 Time interval	9	100	10	
	5 Time interval	10	100	10	

5.3. Mechanical Properties

5.3.1. Compressive Strength (Cast Specimens)

The compressive strength of the designed ECC mixtures was measured and the results of 28 day strength of preliminary tests are presented in Table 10. As displayed in Table 1, eight mixtures with one level of cement substitution (i.e., 50% (wt.), where their C/B wt. ratios are 0.50) by other mineral admixtures (i.e., FA, S, MK, and SF) were studied in this paper. The compressive strength of the ECC mixtures containing standard mixtures and MC-rich ECC mixtures. The compressive strength of ECC standard mixtures and mixtures containing MC are shown in Fig 23 to Fig 26. Each data set for compressive strength at 7, 14, and 28 days is the average of three test results, along with standard deviation. Dark blue columns represent the strength at 7 days, and lighter blue ones are the compressive strength of ECCs at 14 and 28 days. In general, the inclusion of MC (Fig 24.) led to lower compressive strength is comparable to the standard mixtures. Additionally, it is noticeable that replacing cement with slag improved the compressive strength of ECC mixtures compared to fly ash ones. The 28-day strength of the S50 mortar was 68 MPa, which is the highest strength achieved among all mixtures tested (approximately 8% greater than the corresponding strength of the FA50 mortar).

Table 10. Preliminary compressive strength results according to ASTM C39

#	Mix ID	Compressive Strength (MPa) 7-day	Compressive Strength (MPa) 14-day	Compressive Strength (MPa) 28-day
1	FA50- RS36- 0.30%			
2	FA50-0.60%	46.98	55.17	62.70
3	FA50-MC-0.60%	42.53	50.85	55.14
4	FA65- RS39- 0.30%	16.57	20.56	30.81
5	FA75- RS36- 0.13%	16.10	19.71	25.64
6	FA75- RS36- 0.30%	16.62	20.16	-
7	FA75- RS36- 0.40%	15.83	20.04	-
8	FA75-0.60%	26.80	31.72	46.69
9	FA50- 0.30%	35.81	37.00	-
10	FA65- 0.30%	19.66	26.57	-
11	S50-0.60%	51.23	64.37	68.09
12	S50-MC-0.60%	50.11	56.03	59.03
13	S75-0.60%	45.04	52.46	58.94
14	FA25-S50-0.60%	43.86	50.83	55.95
15	FA50-S25-0.60%	37.09	47.94	57.11
16	FA40-SF10-0.60%	40.76	47.92	50.07
17	FA40-SF10-MC-0.60%	42.13	44.67	53.49
18	FA40-MK10-0.60%	45.21	55.59	56.41
19	FA40-MK10-MC-0.60%	47.11	51.33	56.89
20	FA65-SF10-0.60%	24.85	29.23	36.09
21	FA40-S25-SF10-0.60%	31.57	39.58	45.19

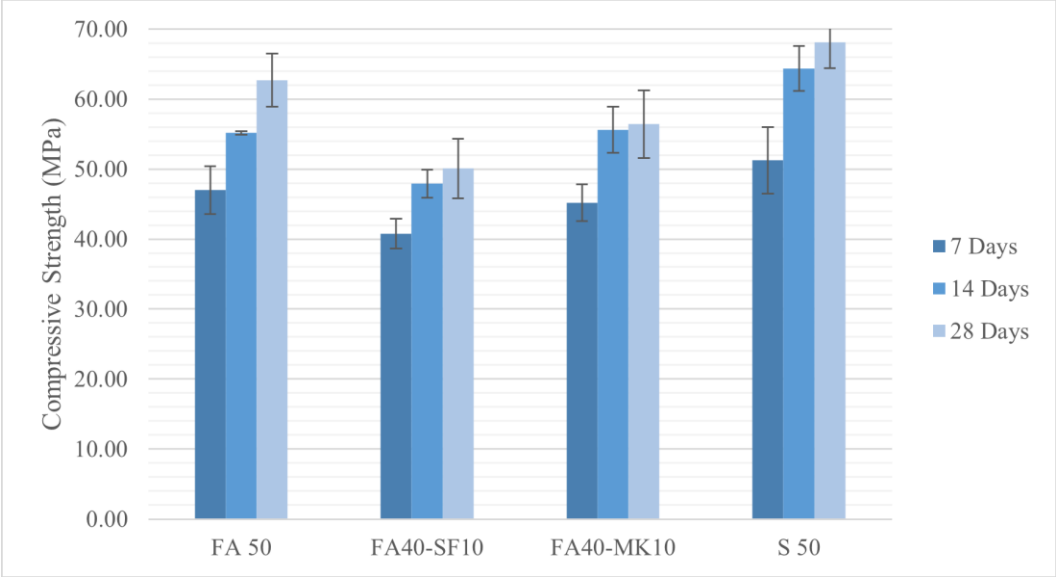


Figure 23. Compressive strength of standard ECC mixtures at 7, 14, and 28 days

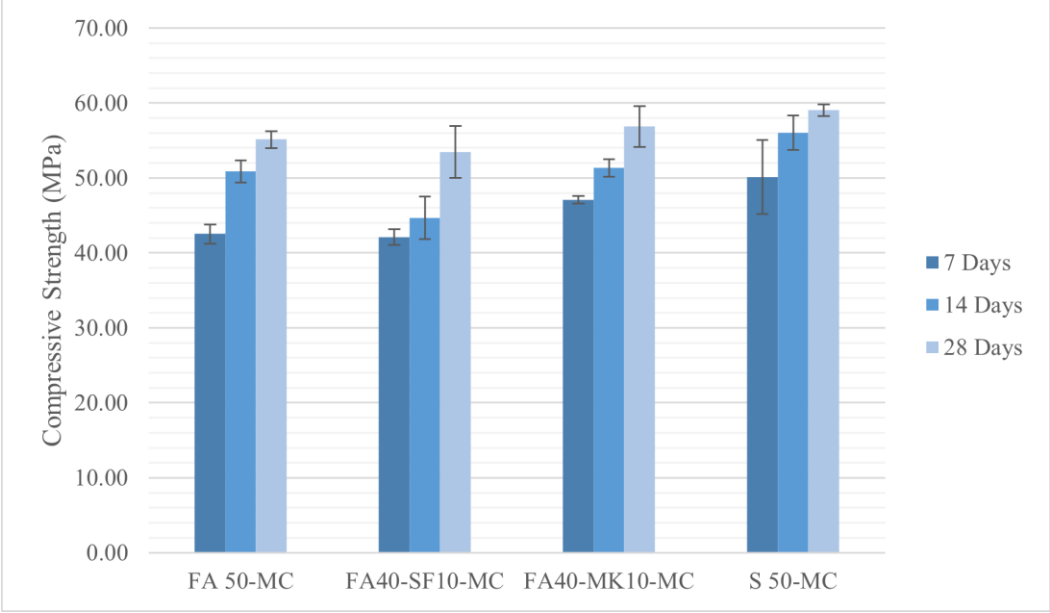


Figure 24. Compressive strength of MC-rich ECC mixtures at 7, 14, and 28 days

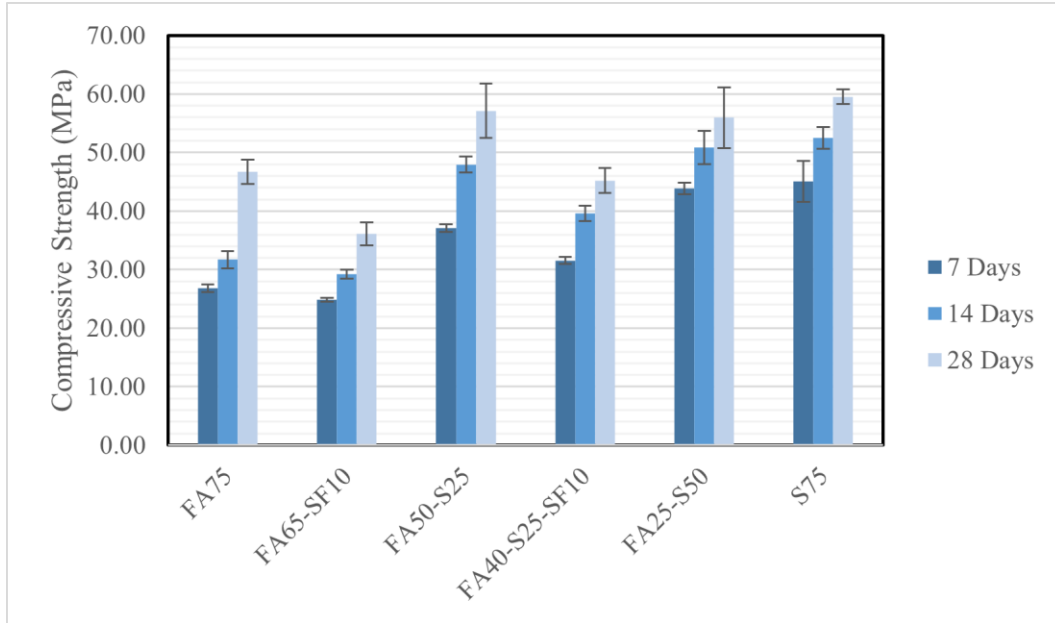


Figure 25. Compressive strength of 75% cement replacement with FA, S, and SF

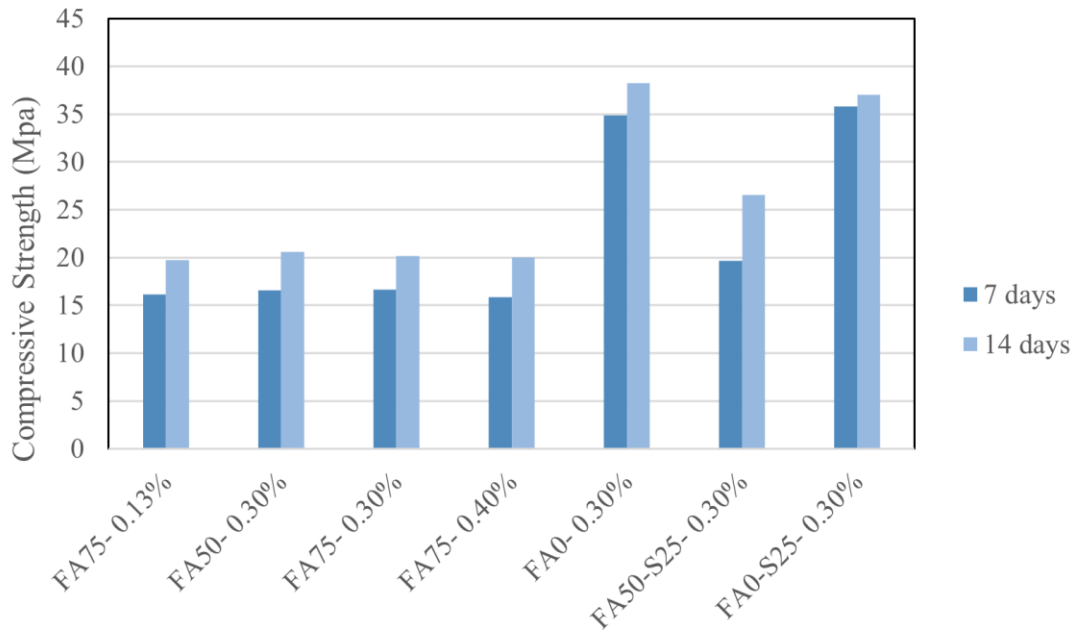


Figure 26. Compressive strength of the Primary mixtures.

5.3.2. Compressive Strength (3D printed specimens)

The compressive strength of 3D printed cubic specimens were also evaluated for 28 days and presented in Fig 27. The compressive strength was found as 35 MPa, 35 MPa, 41 MPa, and 50 MPa for FA50-MC, FA40-SF10-MC, FA40-MK10-MC, and S50-MC respectively. Among all the mixes S50 displayed highest compressive strength even with the incorporation of methylcellulose.

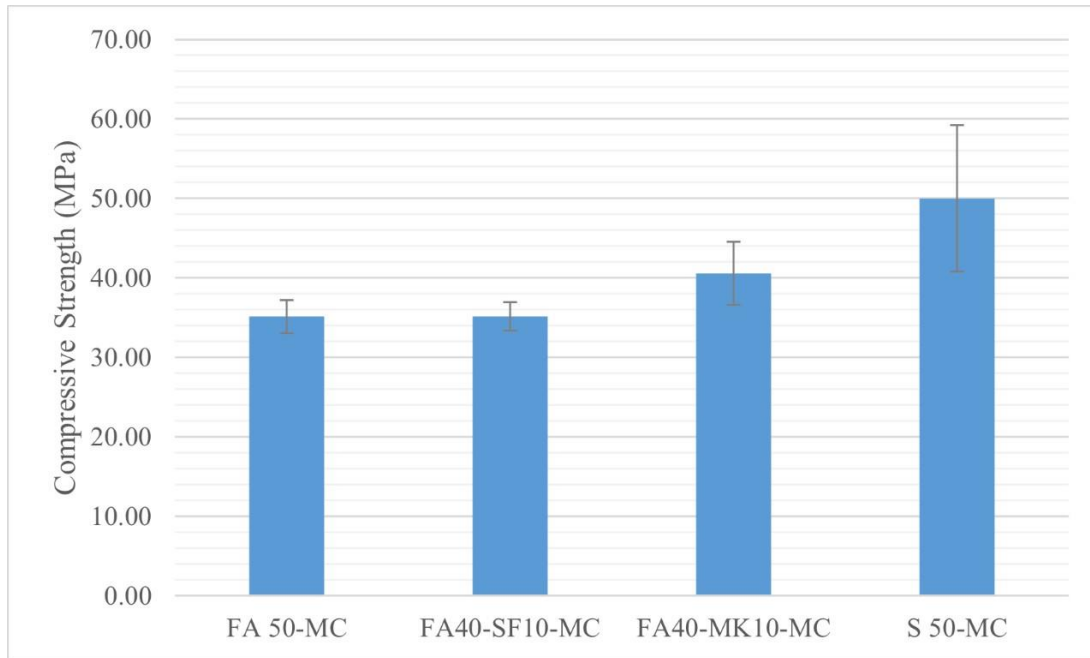


Figure 27. 28 days Compressive strength of the 3D printed specimens

5.3.3. Dry Density

The dry density results at 28 days curing of standard ECC specimen and specimens with incorporation of methylcellulose are presented in Table 11. The results depicted that the dry density showed a decreasing trend when methylcellulose was incorporated in the ECC mixes. The reduction of the compressive strength of MC-enriched mixes can be attributed to the decrease in the dry density.

Table 11. Dry Density of ECC specimens

#	Mix ID	Density (g/cm ³)
1	FA50-0.60%	2.01
2	FA50-MC-0.60%	1.93
3	S50-0.60%	2.03
4	S50-MC-0.60%	1.97
5	FA40-SF10-0.60%	1.80
6	FA40-SF10-MC-0.60%	1.88
7	FA40-MK10-0.60%	1.93
8	FA40-MK10-MC-0.60%	1.91

5.3.4. Direct Tension Test

The direct tension tests were performed, and the results of the tests are presented in Table 12. This test was done with delays because the problems related to the test setup took a long time to be fixed. Since the results of these tests were low and not what the team was expected for the designed mixtures, in the new phase of the Tran Set project, all attempts of the UNM team are focused on improving the mechanical performance by increasing the fiber content, changing the type of fibers and some other strategies which will be presented in the next phase of the project. Additionally, since we didn't achieve the required ductility for designed printable ECC mixtures, the task to evaluate Fracture Properties could not be completed.

Table 12. Preliminary compressive strength results according to ASTM C39

#	Mix ID	Tensile Strength (MPa) 28-day	Ultimate Tensile Strain (%) 28-day
1	FA40-SF10- 0.60%	2.77	2.5
2	FA40-MK10- 0.60%	3.37	1.3
3	FA50-MC-0.60%	4.41	1.8
4	FA40-SF10-MC-0.60%	3.38	1.8
5	FA40-MK10-MC-0.60%	3.31	1.35

5.3.5. Flexural Strength

The flexural strength of two mixtures has been evaluated, for each mixture two specimens has been prepared the results of Peak strength and the deflection at peak strength is presented in figures 28 and 29. The deflection of FA40-SF10 mixture is 21% higher than the FA50. The peak strength of both mixtures is around 1.8 Mpa which is relatively lower than expected. Both the FA40-SF10 and FA10 had a brittle behavior under flexural load.

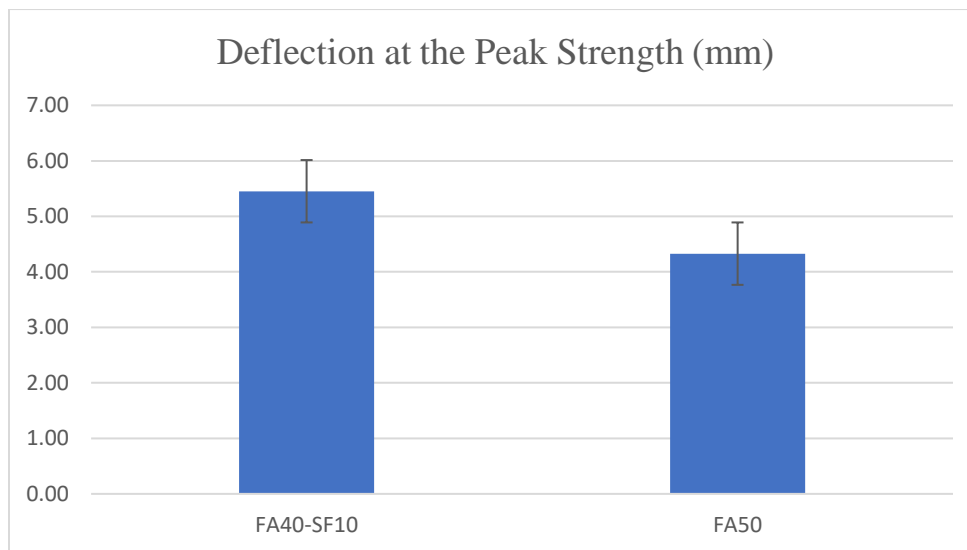


Figure 28. Deflection at the peak strength

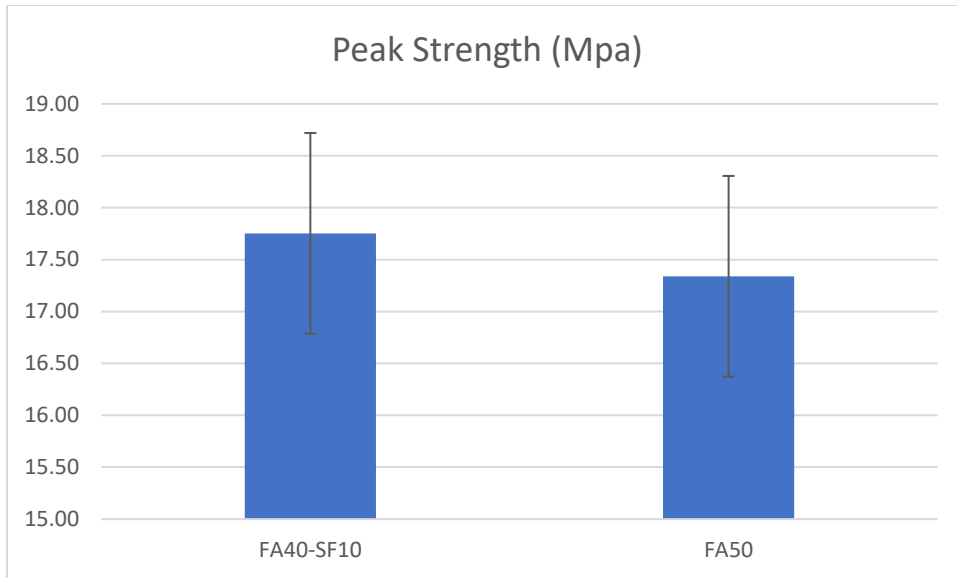


Figure 29. Peak strength of 3D-printed beams

5.3.6. Fracture Properties

As illustrated in Fig 30 the specimens had a single crack in the middle which is a brittle material behavior. The material has not shown sufficient ductility because of which the detail investigation of fracture properties was not worth taking into account. However, in next TranSET project this investigation will be repeated after fixing the issue of the ductility.



Figure 30. Single crack of the beam samples under flexural load.

6. CONCLUSIONS

This study focused on designing 3D printable ECC mixtures by utilizing several supplementary cementitious materials. The ECC mixtures were designed, and their mechanical, rheological, and printing parameters were evaluated. Following conclusions can be drawn from the experimental results:

1. The ECC mixtures improved mechanical behavior (i.e., the maximum compressive strength achieved was 68 MPa, and the corresponding mixture was S50. The other mixtures, FA50, FA40-SF10, and FA40-MK10, have 28 days compressive strength of 62.70 MPa, 50.07 MPa, and 56.41 MPa, respectively.
2. The printing quality with standard ECC mixtures was not satisfactory due to the high content of fibers; the fiber dispersion was not uniform in the mixtures, causing fiber clustering phenomena. Most of the standard ECC mixtures were either collapsed or were not sufficiently extendable.
3. The incorporation of MC as a VMA promoted fibers' dispersion and significantly improved printing quality in dimension conformity, dimension consistency, and shape retention of the printed objects.
4. Although, the addition of MC negatively impacts the mechanical performance as the compressive strength of MC-rich mixtures was relatively lower than the standard ECC mixture, which is also reported in the literature. However, it is still comparable as the maximum strength achieved with MC was 59.03 MPa.
5. The rheological parameters such as plastic viscosity, yield stress, and thixotropy of ECC mixtures with MC were marginally enhanced, another cause of improving extrudability and buildability.
6. The compressive strength of 3D printed specimens will be reported later as the 28 days curing was not completed yet, which will draw a concise comparison of the cast and printed samples strength.
7. The three-point bending test results of 3D printed beams will also be reported later to evaluate flexural strength.
8. The flow table results have given very contrasting information for standard ECC mixtures and mixtures with MC. Some of the standard ECC were not sufficiently extrudable even the flow table value was high. On the contrary, the MC-rich mixtures were extrudable enough even with lower flow table values.

Conclusively, the MC is an efficient viscosity modifying admixture in ECC mixtures as it can improve the printing quality in terms of dimension conformity, dimension consistency, surface quality, buildability, and shape retention with satisfactory mechanical performance.

REFERENCES

1. PCA. Ultra-High Performance Concrete.
2. ASTM C1856. *Standard Practice for Fabricating and Testing Specimens of Ultra-High Performance Concrete*. ASTM International, West Conshohocke, PA, 2017.
3. Yu, K.-Q., J.-T. Yu, J.-G. Dai, Z.-D. Lu, and S. P. Shah. Development of Ultra-High Performance Engineered Cementitious Composites Using Polyethylene (PE) Fibers. *Construction and Building Materials*, Vol. 158, 2018, pp. 217–227. <https://doi.org/10.1016/j.conbuildmat.2017.10.040>.
4. Yu, K., Y. Wang, J. Yu, and S. Xu. A Strain-Hardening Cementitious Composites with the Tensile Capacity up to 8%. *Construction and Building Materials*, Vol. 137, 2017, pp. 410–419. <https://doi.org/10.1016/j.conbuildmat.2017.01.060>.
5. Zhou, Y., B. Xi, K. Yu, L. Sui, and F. Xing. Mechanical Properties of Hybrid Ultra-High Performance Engineered Cementitious Composites Incorporating Steel and Polyethylene Fibers. *Materials*, Vol. 11, No. 8, 2018, p. 1448. <https://doi.org/10.3390/ma11081448>.
6. Hassan, A. M. T., S. W. Jones, and G. H. Mahmud. Experimental Test Methods to Determine the Uniaxial Tensile and Compressive Behaviour of Ultra High Performance Fibre Reinforced Concrete (UHPRFC). *Construction and Building Materials*, Vol. 37, 2012, pp. 874–882. <https://doi.org/10.1016/j.conbuildmat.2012.04.030>.
7. Kim, D. J., K. Wille, A. E. Naaman, and S. El-Tawil. Strength Dependent Tensile Behavior of Strain Hardening Fiber Reinforced Concrete, pp. 3–10.
8. Aghdasi, P., A. E. Heid, and S.-H. Chao. Developing Ultra-High-Performance Fiber-Reinforced Concrete for Large-Scale Structural Applications. *ACI Materials Journal*, Vol. 113, No. 5, 2016. <https://doi.org/10.14359/51689103>.
9. Wille, K., D. J. Kim, and A. E. Naaman. Strain-Hardening UHP-FRC with Low Fiber Contents. *Materials and Structures 2010 44:3*, Vol. 44, No. 3, 2010, pp. 583–598. <https://doi.org/10.1617/S11527-010-9650-4>.
10. Park, S. H., D. J. Kim, G. S. Ryu, and K. T. Koh. Tensile Behavior of Ultra High Performance Hybrid Fiber Reinforced Concrete. *Cement and Concrete Composites*, Vol. 34, No. 2, 2012, pp. 172–184. <https://doi.org/10.1016/j.cemconcomp.2011.09.009>.
11. Chaves Figueiredo, S., C. Romero Rodríguez, Z. Y. Ahmed, D. H. Bos, Y. Xu, T. M. Salet, O. Çopuroğlu, E. Schlangen, and F. P. Bos. An Approach to Develop Printable Strain Hardening Cementitious Composites. *Materials and Design*, Vol. 169, 2019. <https://doi.org/10.1016/j.matdes.2019.107651>.
12. Soltan, D. G., and V. C. Li. A Self-Reinforced Cementitious Composite for Building-Scale 3D Printing. *Cement and Concrete Composites*, Vol. 90, 2018, pp. 1–13. <https://doi.org/10.1016/j.cemconcomp.2018.03.017>.
13. Perrot, A., Y. Mélinge, D. Rangeard, F. Micaelli, P. Estellé, and C. Lanos. Use of Ram Extruder as a Combined Rheo-Tribometer to Study the Behaviour of High Yield Stress Fluids at Low Strain Rate. *Rheologica Acta*, Vol. 51, No. 8, 2012, pp. 743–754. <https://doi.org/10.1007/s00397-012-0638-6>.
14. Wolfs, R. J. M., F. P. Bos, and T. A. M. Salet. Early Age Mechanical Behaviour of 3D Printed Concrete: Numerical Modelling and Experimental Testing. *Cement and Concrete Research*, Vol. 106, 2018, pp. 103–116.
15. Weng, Y., M. Li, Z. Liu, W. Lao, B. Lu, D. Zhang, and M. J. Tan. Printability and Fire Performance

- of a Developed 3D Printable Fibre Reinforced Cementitious Composites under Elevated Temperatures. *Virtual and Physical Prototyping*, Vol. 14, No. 3, 2019, pp. 284–292. <https://doi.org/10.1080/17452759.2018.1555046>.
16. Kazemian, A., X. Yuan, E. Cochran, and B. Khoshnevis. Cementitious Materials for Construction-Scale 3D Printing: Laboratory Testing of Fresh Printing Mixture. *Construction and Building Materials*, Vol. 145, 2017, pp. 639–647.
 17. Albar, A., M. Chougan, M. J. Al- Kheetan, M. R. Swash, and S. H. Ghaffar. Effective Extrusion-Based 3D Printing System Design for Cementitious-Based Materials. *Results in Engineering*, Vol. 6, 2020. <https://doi.org/10.1016/j.rineng.2020.100135>.
 18. Roussel, N., J. Spangenberg, J. Wallevik, and R. Wolfs. Numerical Simulations of Concrete Processing: From Standard Formative Casting to Additive Manufacturing. *Cement and Concrete Research*, Vol. 135, No. April, 2020, p. 106075. <https://doi.org/10.1016/j.cemconres.2020.106075>.
 19. Li, V. *Engineered Cementitious Composites (ECC): Bendable Concrete for Sustainable and Resilient Infrastructure*. 2019.
 20. Li, V. C. Engineered Cementitious Composite (Ecc): Material, Structural, and Durability Performance. *Concrete Construction Engineering Handbook, Second Edition*, 2008, pp. 1001–1048.
 21. Weimann, M. B., and V. C. Li. Hygral Behavior of Engineered Cementitious Composites (ECC). *International Journal for Restoration of Buildings and Monuments*, Vol. 9, No. 5, 2003, pp. 513–534.
 22. Li VC, L. C. Theory of Steady State and Multiple Cracking of Random Discontinuous Fiber Reinforced Brittle Matrix Composites. *Eng Mech-ASCE*, Vol. 118, No. 11, 1992, pp. 2246–64.
 23. Yang, E. H., S. Wang, Y. Yang, and V. C. Li. Fiber-Bridging Constitutive Law of Engineered Cementitious Composites. *Journal of Advanced Concrete Technology*, Vol. 6, No. 1, 2008, pp. 181–193. <https://doi.org/10.3151/jact.6.181>.
 24. Ranade, R. Advanced Cementitious Composite Development for Resilient and Sustainable Infrastructure. PhD Thesis. 2014, p. 419.
 25. Li, V. C. *Engineered Cementitious Composites (ECC)*. Springer Berlin Heidelberg, Berlin, Heidelberg, 2019.
 26. Marchon, D., S. Kawashima, H. Bessaies-Bey, S. Mantellato, and S. Ng. Hydration and Rheology Control of Concrete for Digital Fabrication: Potential Admixtures and Cement Chemistry. *Cement and Concrete Research*, Vol. 112, No. December 2017, 2018, pp. 96–110. <https://doi.org/10.1016/j.cemconres.2018.05.014>.
 27. Li, V. C., F. P. Bos, K. Yu, W. McGee, T. Y. Ng, S. C. Figueiredo, K. Nefs, V. Mechtcherine, V. N. Nerella, J. Pan, G. P. A. G. van Zijl, and P. J. Kruger. On the Emergence of 3D Printable Engineered, Strain Hardening Cementitious Composites (ECC/SHCC). *Cement and Concrete Research*, Vol. 132, No. January, 2020, p. 106038. <https://doi.org/10.1016/j.cemconres.2020.106038>.
 28. Li, Z., M. Hojati, Z. Wu, J. Piasente, N. Ashrafi, J. P. Duarte, S. Nazarian, S. G. Bilén, A. M. Memari, and A. Radlińska. Fresh and Hardened Properties of Extrusion-Based 3D-Printed Cementitious Materials: A Review. *Sustainability (Switzerland)*, Vol. 12, No. 14, 2020, pp. 1–33. <https://doi.org/10.3390/su12145628>.
 29. Roussel, N. Rheological Requirements for Printable Concretes. *Cement and Concrete Research*, Vol. 112, 2018, pp. 76–85.
 30. Lim, S., R. A. Buswell, T. T. Le, S. A. Austin, A. G. F. Gibb, and T. Thorpe. Developments in

- Construction-Scale Additive Manufacturing Processes. *Automation in Construction*, Vol. 21, No. 1, 2012, pp. 262–268. <https://doi.org/10.1016/j.autcon.2011.06.010>.
31. Le, T. T., S. A. Austin, S. Lim, R. A. Buswell, A. G. F. Gibb, and T. Thorpe. Mix Design and Fresh Properties for High-Performance Printing Concrete. *Materials and Structures/Materiaux et Constructions*, Vol. 45, No. 8, 2012, pp. 1221–1232. <https://doi.org/10.1617/s11527-012-9828-z>.
 32. Malaeb, Z., H. Hachem, A. Tourbah, T. Maalouf, N. El Zarwi, and F. Hamzeh. 3D Concrete Printing: Machine and Mix Design. *International Journal of Civil Engineering and Technology*, Vol. 6, No. April, 2015, pp. 14–22.
 33. Ma, G. W., L. Wang, and Y. Ju. State-of-the-Art of 3D Printing Technology of Cementitious Material—An Emerging Technique for Construction. *Science China Technological Sciences*, Vol. 61, No. 4, 2018, pp. 475–495. <https://doi.org/10.1007/s11431-016-9077-7>.
 34. Zhang, Y., Y. Zhang, G. Liu, Y. Yang, M. Wu, and B. Pang. Fresh Properties of a Novel 3D Printing Concrete Ink. *Construction and Building Materials*, Vol. 174, 2018, pp. 263–271. <https://doi.org/10.1016/j.conbuildmat.2018.04.115>.
 35. Ding, Y., J. tao Yu, K. Q. Yu, and S. lang Xu. Basic Mechanical Properties of Ultra-High Ductility Cementitious Composites: From 40 MPa to 120 MPa. *Composite Structures*, Vol. 185, 2018, pp. 634–645. <https://doi.org/10.1016/j.compstruct.2017.11.034>.
 36. Curosu, I., V. Mechtcherine, and O. Millon. Effect of Fiber Properties and Matrix Composition on the Tensile Behavior of Strain-Hardening Cement-Based Composites (SHCCs) Subject to Impact Loading. *Cement and Concrete Research*, Vol. 82, 2016, pp. 23–35. <https://doi.org/10.1016/j.cemconres.2015.12.008>.
 37. Lei, D. Y., and L. P. Guo. Physical and Mechanical Properties of Ultra-High Strength and High Ductility Cementitious Composites. No. 15, 2018, pp. 211–220.
 38. Ogura, H., V. N. Nerella, and V. Mechtcherine. Developing and Testing of Strain-Hardening Cement-Based Composites (SHCC) in the Context of 3D-Printing. *Materials*, Vol. 11, No. 8, 2018. <https://doi.org/10.3390/ma11081375>.
 39. Zhu, Y., Z. Zhang, Y. Yang, and Y. Yao. Measurement and Correlation of Ductility and Compressive Strength for Engineered Cementitious Composites (ECC) Produced by Binary and Ternary Systems of Binder Materials: Fly Ash, Slag, Silica Fume and Cement. *Construction and Building Materials*, Vol. 68, 2014, pp. 192–198. <https://doi.org/10.1016/j.conbuildmat.2014.06.080>.
 40. Chen, J. J., W. W. S. Fung, and A. K. H. Kwan. Effects of CSF on Strength, Rheology and Cohesiveness of Cement Paste. *Construction and Building Materials*, Vol. 35, 2012, pp. 979–987. <https://doi.org/10.1016/j.conbuildmat.2012.04.037>.
 41. Bao, Y., M. Xu, D. Soltan, T. Xia, A. Shih, H. L. Clack, and V. C. Li. Three-Dimensional Printing Multifunctional Engineered Cementitious Composites (ECC) for Structural Elements. *RILEM Bookseries*, Vol. 19, 2019, pp. 115–128. https://doi.org/10.1007/978-3-319-99519-9_11.
 42. Zhu, B., J. Pan, B. Nematollahi, Z. Zhou, Y. Zhang, and J. Sanjayan. Development of 3D Printable Engineered Cementitious Composites with Ultra-High Tensile Ductility for Digital Construction. *Materials and Design*, Vol. 181, 2019, p. 108088. <https://doi.org/10.1016/j.matdes.2019.108088>.
 43. Heikal, M., and N. S. Ibrahim. Hydration, Microstructure and Phase Composition of Composite Cements Containing Nano-Clay. *Construction and Building Materials*, Vol. 112, 2016, pp. 19–27. <https://doi.org/10.1016/j.conbuildmat.2016.02.177>.
 44. Tregger, N. A., M. E. Pakula, and S. P. Shah. Influence of Clays on the Rheology of Cement Pastes. *Cement and Concrete Research*, Vol. 40, No. 3, 2010, pp. 384–391.

45. Yang, E. H., Y. Yang, and V. C. Li. Use of High Volumes of Fly Ash to Improve ECC Mechanical Properties and Material Greenness. *ACI Materials Journal*, Vol. 104, No. 6, 2007, pp. 620–628. <https://doi.org/10.14359/18966>.
46. Noorvand, H., G. Arce, M. Hassan, T. Rupnow, and L. N. Mohammad. Investigation of the Mechanical Properties of Engineered Cementitious Composites with Low Fiber Content and with Crumb Rubber and High Fly Ash Content. *Transportation Research Record*, Vol. 2673, No. 5, 2019, pp. 418–428. <https://doi.org/10.1177/0361198119837510>.
47. Mechtcherine, V., J. Grafe, V. N. Nerella, E. Spaniol, and M. Hertel. 3D-Printed Steel Reinforcement for Digital Concrete Construction – Manufacture , Mechanical Properties and Bond Behaviour. *Construction and Building Materials*, Vol. 179, 2018, pp. 125–137. <https://doi.org/10.1016/j.conbuildmat.2018.05.202>.
48. Hack, N., T. Wangler, J. Mata-Falcón, K. Dörfler, N. Kumar, A. N. Walzer, K. Graser, L. Reiter, H. Richner, J. Buchli, W. Kaufmann, R. J. Flatt, F. Gramazio, and M. Kohler. Mesh Mould: An on Site, Robotically Fabricated, Funtional Formwork: Konferenzbeitrag. *Second Concrete Innovation Conference (2nd CIC)*, No. March, 2017.
49. Salet, T. A. M., Z. Y. Ahmed, F. P. Bos, and H. L. M. Laagland. Design of a 3D Printed Concrete Bridge by Testing Design of a 3D Printed Concrete Bridge by Testing. *Virtual and Physical Prototyping*, Vol. 0, No. 0, 2021, pp. 1–15. <https://doi.org/10.1080/17452759.2018.1476064>.
50. ASTM C305 - 14. *Standard Practice for Mechanical Mixing of Hydraulic Cement Pastes and Mortars of Plastic Consistency*. ASTM International, West Conshohocken, PA, 2014.
51. Zhang, D., and B. Wei, Eds. *Mechatronics and Robotics Engineering for Advanced and Intelligent Manufacturing*. Springer International Publishing, Cham, 2017.
52. ASTM C125 - 20. *Standard Terminology Relating to Concrete and Concrete Aggregates*. ASTM International, West Conshohocken, PA, 2020.
53. Panda, B., and M. J. Tan. Experimental Study on Mix Proportion and Fresh Properties of Fly Ash Based Geopolymer for 3D Concrete Printing. *Ceramics International*, Vol. 44, No. 9, 2018, pp. 10258–10265. <https://doi.org/10.1016/j.ceramint.2018.03.031>.
54. Panda, B., S. Ruan, C. Unluer, and M. J. Tan. Improving the 3D Printability of High Volume Fly Ash Mixtures via the Use of Nano Attapulgite Clay. *Composites Part B: Engineering*, Vol. 165, No. November 2018, 2019, pp. 75–83. <https://doi.org/10.1016/j.compositesb.2018.11.109>.
55. ASTM C191 -19. *ASTM C191 - 19 Standard Test Methods for Time of Setting of Hydraulic Cement by Vicat Needle*. ASTM International, West Conshohocken, PA, 2019.
56. ASTM C1437 - 15. *Standard Test Method for Flow of Hydraulic Cement Mortar*. ASTM International, West Conshohocken, PA, 2015.
57. Weltmann, R. N., and H. Green. Rheological Properties of Colloidal Solutions, Pigment Suspensions, and Oil Mixtures. *Journal of Applied Physics*, Vol. 14, No. 11, 1943, pp. 569–576.
58. Long, W.-J., J.-L. Tao, C. Lin, Y. Gu, L. Mei, H.-B. Duan, and F. Xing. Rheology and Buildability of Sustainable Cement-Based Composites Containing Micro-Crystalline Cellulose for 3D-Printing. *Journal of Cleaner Production*, Vol. 239, 2019, p. 118054. <https://doi.org/10.1016/j.jclepro.2019.118054>.
59. ASTM C1609-19. *Standard Test Method for Flexural Performance of Fiber-Reinforced Concrete (Using Beam With Third-Point Loading)*. ASTM International, West Conshohocken, PA, 2019.
60. Yuan, K., L. Liao, Y. Wang, Z. Zhang, D. Chen, and C. Wang. Individual and Combined Effects of Modified Starch, Bentonite and Their Composite Powder with HPMC on the Performance of

Cement Mortars. *Journal of Polymer Engineering*, Vol. 33, No. 6, 2013, pp. 551–555.

APPENDIX A: Technical Parameters of 3D-Printer

Cartesian Coordinate 3D-Printer Technical Parameters

Technical parameters of JYHC 3D printing gantry robot system (3DPRT)		
Frame structure	Size: length (mm) * width (mm) * height (mm)	2800*2010*2600
	Weight (Kg)	300
	Drive motor	Stepper motor, five
	Power supply	AC 220V
Mixing and feeding system	Shear mixer Capacity(L) Voltage (V) Power (W) Weight (Kg)	50 (recommended) (max 60) 380 AC 3000 300x2
	Pumping system Voltage (V) Power (W) Horizontal transmission distance(M) Transmission height (m) Weight (Kg)	380 AC 4000 15 5 180
	Transporting pipe: Material Length(m) Inner diameter(mm)	Rubber 5 45
Motion control system	Effective size : length (mm) *width (mm) *height (mm)	1800*1600*1800
	XY Plane moving speed (mm/s)	10 to 350
	Z moving speed (mm/S)	10 to 20
Printing head	Diameter of printing head (mm)	25, 35, 45 mm
	The diameter of Acrylic printing head (mm)	40 mm
	Ways of adding material	Manual (through the printing head) or automatic (pumping system)
Software	Software development environment	LabVIEW (reads from a G-Code)
	Interface text	English
	Software upgrade	Network transmission, Free of renew